Interfacing Dynamic Phasor Based System Equivalents to an Electromagnetic Transient Simulation

By:
Konara Mudiyanselage Harshani
Koushalya Konara

A Thesis submitted to the Faculty of Graduate Studies of The University of Manitoba in partial fulfilment of the requirements of the degree of

MASTER OF SCIENCE

Department of Electrical and Computer Engineering
University of Manitoba
Winnipeg

Abstract

This thesis presents a method to do transient simulation of a large power system using dynamic phasors and electromagnetic transient simulation. A novel hybrid simulation technique using dynamic phasor equivalent is presented to analyse a part of a large power system. Electromagnetic transient simulation is used to model the part of the network that needs detailed simulation. The synchronous reference frame phase locked loop is implemented as the interface between the electromagnetic transient model and the dynamic phasor model. Two types of positive sequence filters i) sinusoidal signal integrator phase locked loop ii) extended phase locked loop are presented to eliminate the voltage unbalance effect in a phase locked loop. A comparison of the performance of the two filters is presented. The validation of the proposed interface is done using EMT simulation on real time digital simulator. Finally the numerical problems involved in this hybrid method are discussed.

Acknowledgements

Firstly, I would like to express my sincere gratitude to my advisor Prof. U. D. Annakkage for the continuous support for my Master's Degree. It has been an honour and a privilege to work under you. I could not have imagined having a better advisor and mentor for my graduate studies.

I'm very much thankful to Dr. Chandana Karawita for showing interest on my research and his valuable suggestions received. I would also like to thank the examining committee for taking their valuable time to read this thesis. I thank my graduate advisor Amy Dario for her support.

I like to thank Prof. Athula Rajapakse and Prof. Aniruddha Gole for the invaluable knowledge they shared during the course work. I thank my research group mates for the stimulating discussions and for all the fun we have had in the last two years.

A very special thank you goes to my sister Anupama Konara, for encouraging me to pursue a graduate degree. You offered invaluable support over the years. I also like to thank my brother-in-law for the support and encouragement received.

I would like to thank all my friends in Winnipeg for their support during these two years. A special thank goes to Annakkage family for their caring and concern.

I would like to extend my deepest gratitude to my parents. Without their encouragement, I would not have a chance to achieve this much. I would also like to thank my brother for constantly reminding me what I should accomplish.

Finally, I would like to thank my husband Sampath, who stood by me through the good times and bad.

Contents

List of Tables

List of Figures

Abbreviations

EMT	**E**lectro **M**agnetic **T**ransient
EMTP	**E**lectromagnetic **T**ransient **P**rogram
TSP	**T**ransient **S**tability **P**rogram
DP	**D**ynamic **P**hasors
PLL	**P**hase **L**ocked **L**oop
SRF-PLL	**S**ynchronous **R**eference **F**rame **P**hase **L**ocked **L**oop
RTDS	**R**eal **T**ime **D**igital **S**imulator
IEEE	**I**nstitution of **E**lectrical and **E**lectronic **E**ngineers
FDNE	**F**requency **D**ependant **N**etwork **E**quivalent
TLNE	**T**wo **L**ayer **N**etwork **E**quivalent
FACTS	**F**lexible **AC** **T**ransmission **S**ystems
PI	**P**ropotional - **I**ntegral

Symbols

t	Time
Δt	Time step
j	Imaginary unit
V	Voltage
I	Current
v	Instantaneous voltage
i	instantaneous current
V_R, V_I	Real and imaginary components of AC bus voltage
I_R, I_I	Real and imaginary components of AC current
V_m	Magnitude of the voltage
I_{dy}	Injected current from the dynamic phasor model
RL	Resistor and inductor
RC	Resistor and capacitor
ω_0	Fundamental angular frequency
$[Y]$	Admittance matrix of a network
$[Y]^{-1}$	Inverse of the admittance matrix of a network
$[A]$	System Matrix of a state space model
$[B]$	Input Matrix of a state space model
k_p	Proportional gain
k_i	Integral gain
V_{a0}, V_{b0}, V_{c0}	Zero sequence components of three phase voltages

V_{a1}, V_{b1}, V_{c1}	Positive sequence components of three phase voltages
V_{a2}, V_{b2}, V_{c2}	Negative sequence components of three phase voltages
k	Filter gain of the SSI-PLL

To my family and friends.

Chapter 1

Introduction

1.1 Problem Definition

The power system of today is a complex interconnected system containing thousands of buses and a large number of power system components. Computer-based simulation programs are necessary to model these large scale power systems and the interdependencies among their components. The dynamics of the power system take different periods of time due to its complexity. The time scale of power system transients can vary from micro-seconds to days. Figure 1.1 shows typical time ranges for different dynamics in a power system [1].

Power system transients can be divided into two categories based on the time scale: electromagnetic transients and electromechanical transients. The electromagnetic transients take place due to the interactions between magnetic fields of the inductances and the electric fields of the capacitances in the system. The electromechanical transients are the results of the interaction between the mechanical energy stored in the rotating machines. The region in the middle of Figure

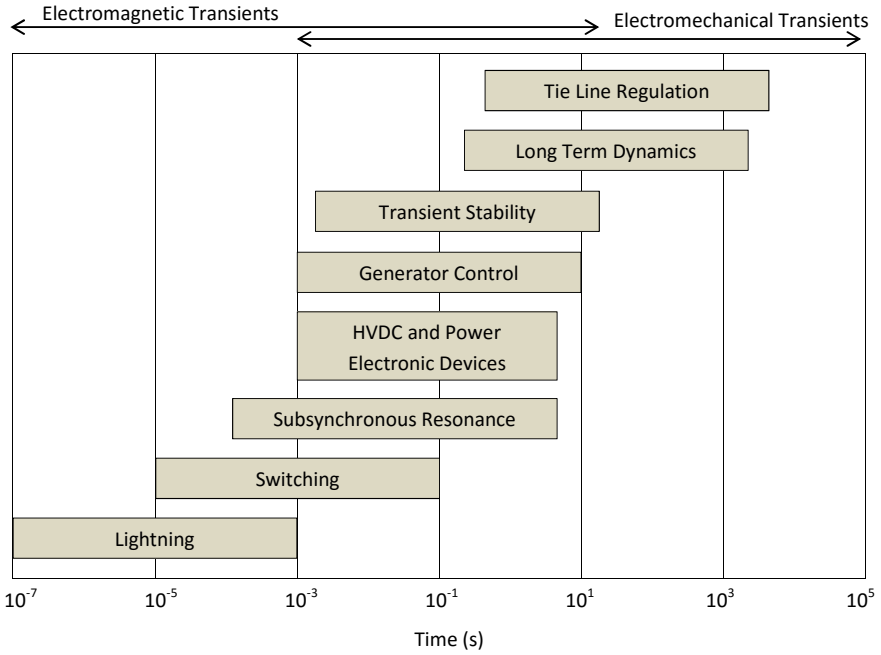

FIGURE 1.1: Time scale of different power system transients

1.1 represents the transient stability region where both the electromechanical and the electromagnetic transients play a role.

Different types of power system simulation models are required to study different regions of power system dynamics. Fast electromagnetic transients are studied using electromagnetic transient programs (EMTP) with a small time step (typically 50μs or less) to cover the required bandwidth. The size of the time step depends on the type of the electromagnetic transient under study. In EMT simulation, power system components are adequately modelled to simulate high frequency transients. However, use of EMTP is not practical to analyse large power systems since it uses a very small time step.

Transient stability programs (TSP) are typically used to analyse slow electromechanical transients. It uses phasor models of transmission lines and simplified rotating machine models. It neglects fast electromagnetic transients and

assumes that the power transfer takes place at the system frequency. It uses a larger time step (half a cycle) enabling the TSP simulation to solve large power systems to simulate slow electromechanical transients [2]. Due to its nature, transient stability models can never capture the fast dynamics of a power system. On the other hand, EMT type simulations can be used to analyse slow electromechanical transients but it is impractical due to following reasons [3].

- Transient stability type simulation is usually used for simulating large power systems. However the EMT model will require lot of computational power to handle large power systems and it is practically impossible.
- Due to the longer time span of electromechanical transients the simulation has to be carried out for a longer period of time.
- Due to the small time step of the EMTP high computational power will be required.

For these reasons, EMT programs are impractical for simulation of large systems. However on the other hand transient stability programs cannot represent certain individual components of the system in detail such as power electronic devices. Therefore, integrated approaches are necessary when analysing large power systems. When EMT type simulations are used to simulate large power systems, common practice is to divide the system into two zones. The zone where the transient phenomena occur (zone 1) is modelled using the detailed EMT type simulation and the rest of the system (zone 2) is modelled using phasor-type simulation [2]. In this study the zone 1 will be called as the internal system and the zone 2 will be called as the external system.

1.2 Background

In this section available techniques for analysing large power systems are discussed, the concept of hybrid simulator is studied and interfacing of TSP to EMTP is discussed. Alternative methods to analyse both electromagnetic and electromechanical transients in a large system are also presented.

1.2.1 TSP and EMT Hybrid Simulation

In hybrid simulation, since the EMT type simulation needs more computational power compared to transient stability program only the components that need detailed simulation are modelled using the EMT model and the rest of the system is modelled as a Thevenin's equivalent circuit using TSP [4]. However, this method does not adequately model the high frequency response of the external system. Therefore, to model the external system in the EMT model, a dynamic equivalent model that accurately represent the external system is required [2].

Therefore, when modelling the external system, there should be a suitable technique to determine dynamic equivalent models that accurately represent the external system to the EMT model. The dynamic equivalent of the external system can be divided into three categories.

1. To investigate high frequency transients transmission lines should be modelled to reflect the frequency dependency. This can be further classified into frequency dependent network equivalents (FDNE), and two layer network equivalents (TLNE).

   (i) Frequency Dependent Network Equivalents (FDNE): A more complex Thevenin's impedance is used to represent the external system, which

not only represents the external system at the fundamental frequency but also at a selected range of harmonic frequencies [5].

(ii) Two Layer Network Equivalents (TLNE): When the external system becomes larger, the order of the FDNE filter increases. This will increase the computational power required. In TLNE, the external system is divided into two parts: a surface-layer containing low-order frequency-dependent transmission lines and a deep region containing the low-order FDNE model [6].

2. To study low frequency electromechanical oscillations, the transmission lines can be modelled as constant impedances and the generators can be modelled neglecting the stator winding transients.

3. To study subsynchronous oscillations, the turbine-generator dynamics and network transients must be adequately modelled.

The representation of the external system using FDNE network involves some complications. Some of these are summarized below.

- Coming up with a stable FDNE model for a large multi-port external system is difficult.
- The resultant FDNE model should preserve stability, passivity and causality which will lead to a numerically stable simulation [7].
- The FDNE model should not change the behaviour of the original network.

Considering the above limitations it can be stated that design of the FDNE filter for a particular system involves complications, and it can also decrease the accuracy of the entire simulation.

1.2.2 Alternative Methods of Analysing Large Power Systems

Another method of simulating both electromagnetic and electromechanical transients is to use of the concept of dynamic phasors [3]. Some advantages of using dynamic phasor simulation are mentioned below [8]. More details on dynamic phasor models will be discussed on Section 2.2 of Chapter 2.

- Dynamic phasor model can capture the network dynamics of the power system.
- Dynamic phasors can be used to compute fast electromagnetic transients with larger step size [9].
- It allows model simplification to reduce the order of the dynamic phasor model.

Some limitations of this method would be,

- Dynamic phasor models are not accurate when the center frequency of the simulation changes.
- Frequency range that the dynamic phasors can model is less compared to EMTP.
- Dynamic phasors assume balanced operation.

Therefore, the need for a simulation tool that is capable of simulating the electromagnetic and electromechanical transients adequately in one simulation is required. The aim of this study is to develop a simulation technique using dynamic phasor equivalent to represent the external system of a large power system and

integrate it to an EMT simulation [10]. The resultant model with the external system modelled using dynamic phasors is compared against the fully EMT model.

1.3 Thesis Outline

This thesis presents a new method to simulate a large power system using dynamic phasor equivalent and electromagnetic transient simulation. At the beginning of this chapter the available techniques to analyse a large power system have been discussed and the limitations of these methods have been pointed out.

In Chapter 2, a discussion on EMT simulation and the dynamic phasor model is presented. Derivation of basic circuit models using EMT simulation model is also presented. An introduction to the hybrid simulation using dynamic phasors and EMT model is given.

The basic equations for a RL and RC circuit are derived using dynamic phasors in Chapter 3. Two sets of equations are presented using state space analysis and nodal analysis.

Interfacing dynamic phasor equivalent to the EMT type simulation is presented in Chapter 4. Synchronous reference frame phase locked loop is proposed as the interface between the two models. A comparison of results of the hybrid phasor model and the EMT model is also presented in this chapter.

In Chapter 5, two positive sequence filters for improving the SRF-PLL performance in a voltage unbalance situation is presented. The two methods discussed are the sinusoidal signal integrator PLL and the extended PLL. A comparison of the performance of the two positive sequence filters is also presented.

In Chapter 6, the work involved in implementing the proposed hybrid system in real time digital simulator is presented. Difficulties of implementing this process is also discussed.

Chapter 7 summarises the contribution and the conclusion of this work along with some suggestions for future research.

Chapter 2

Simulations Models of Power Systems

2.1 Electromagnetic Transient Simulation

Electromagnetic transient simulation (EMT) has become an important tool for analysing fast electromagnetic transients in a power system. It models the power system in detail to analyse voltage spikes, current surges, harmonics etc. [1]. State-space and nodal analysis approaches are the most widely used methods for carrying out electromagnetic transient simulation [11]. In the state space approach a power system of order n is expressed using n number of differential equations (state equations). One downside of this method is that the algorithm becomes complex when handling large networks (for larger power systems the required number of state equations is high). Therefore, in an automated digitalized solution it is hard to generalize the program to come up with the system's state equations.

Today, many EMT based simulation softwares adopt a method based

on nodal analysis developed by H. W. Dommel. This method can be considered as the most widely used method to model electromagnetic transients. In this method, each of the power system component is represented as a Norton equivalent circuit. The differential equations are solved to obtain a generalized solution using numerical integration. Then this solution is represented using a current source (derived from the past values) and a resistor parallel to it (the Norton equivalent). Since each component is modelled separately, it is easy to obtain a generalized solution using nodal analysis, which needs fewer details of the network topology. Later a set of nodal equations can be derived using each Norton equivalent to solve the network and to come up with the node voltages. This concept is described in the next section.

2.1.1 Nodal Analysis

The nodal analysis approach is a step by step approach where a set of equations is solved in each time step (Δt). Before starting the simulation all the components are modelled as a current source-conductance equivalents, and the admittance matrix ($[Y]$) of the resultant network is obtained. The simulation starts with some initial values which are used to update the value of the current sources at the beginning of the simulation. Then, the network is solved using Kirchoff's current law and new voltages are derived using (2.1) and (2.2), where J is derived from real current sources and $I(t - \Delta t)$ is derived from fictitious current sources (history terms) in the network. Here the term "$[Y]^{-1}$" is the inverse of the admittance matrix of the network.

$$[Y]V = J + I(t - \Delta t) \tag{2.1}$$

$$V = [Y]^{-1}[J + I(t - \Delta t)] \tag{2.2}$$

The history terms (value of the fictitious current sources) is then updated in the next time step using the past values of the voltages. This procedure is carried out until the end of simulation. The flow chart of the process is shown in Figure 2.1.

Numerical Integration

To model simple components such as capacitors, inductors or more complex non linear components (e.g., saturable inductors) using nodal analysis, the component must be represented using its Norton equivalent circuit. For most of the components the Norton equivalent circuit can be derived using numerical integration methods. A number of integration methods can be used for this purpose such as forward/backward Euler method, second-order Runge Kutta integration, fourth-order Runge Kutta integration, trapezoidal integration, etc. Among these methods, the trapezoidal rule of integration is used in most of the simulation programs since it preserves stability for linear systems. Trapezoidal rule is accurate, numerically stable, and simple. Consider a first-order differential equation of the following form:

$$\frac{dx}{dt} = f(x,t) \tag{2.3}$$

According to Figure 2.2,

$$x_1 = x_0 + \int_{t_0}^{t_1} f(x,t)d\tau \tag{2.4}$$

Using the trapezoidal rule of integration,

$$x_1 = x_0 + \frac{\Delta t}{2}\big(f(x_0,t_0) + f(x_1,t_1)\big) \tag{2.5}$$

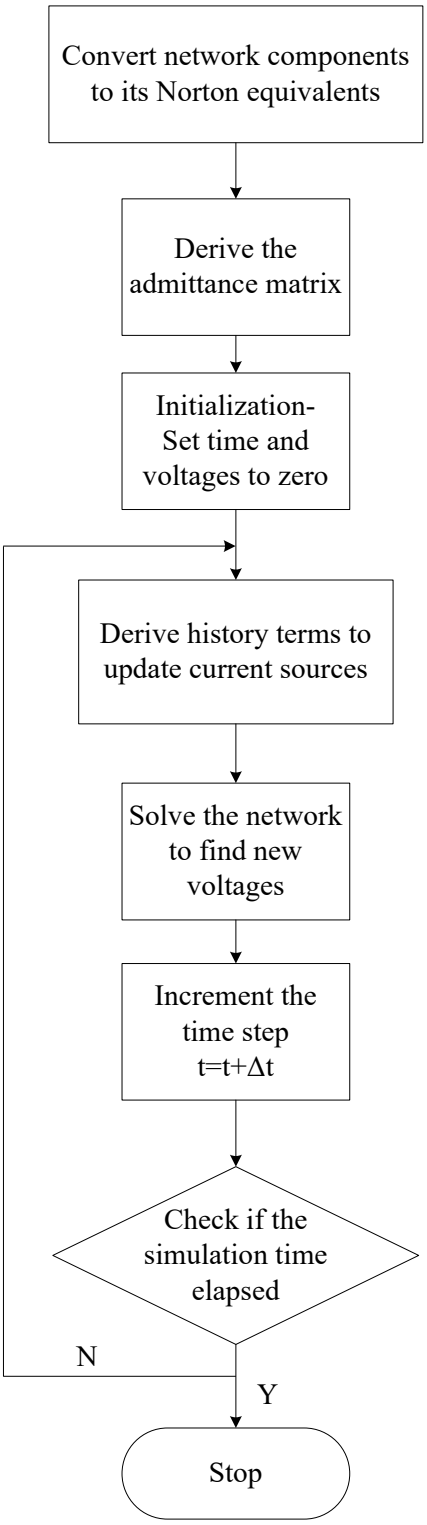

FIGURE 2.1: The simulation steps of nodal analysis in EMT simulation

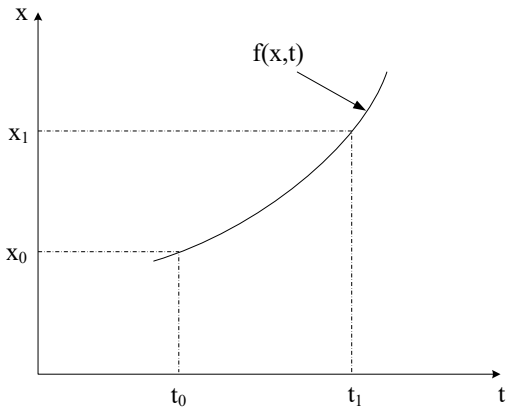

FIGURE 2.2: Numerical integration using trapezoidal rule

In general,

$$x_{n+1} = x_n + \frac{\Delta t}{2}\big(f(x_n, t_n) + f(x_{n+1}, t_{n+1})\big) \tag{2.6}$$

These sets of equations can be used to determine the Norton equivalent circuit for a given component. The derivation of Norton equivalent circuit for an inductor and a capacitor is given below as examples.

Modelling an Inductor using Dommel's Algorithm

In (2.7), the differential equation governing the voltage-current relationship for an inductor is shown. The derivation of the Norton equivalent circuit, starting from this basic equation is shown below.

$$\frac{d}{dt}i = \frac{1}{L}v \tag{2.7}$$

where, L is the inductance, i is the current through the inductor and v is the voltage between the inductor. Here, lower-case v and i represent the instantaneous voltages and currents.

Applying trapezoidal rule of integration to the above equation results in (2.9), where $I_L(t-\Delta t)$ is the history term, which can be regarded as the current source of the Norton equivalent. The term g_L can be regarded as the conductance parallel with the current source. The equivalent circuit of the inductor is shown in Figure 2.3.

$$i(t) = i(t-\Delta t) + \frac{\Delta t}{2L}\Big[v(t-\Delta t) + v(t)\Big] \tag{2.8}$$

$$i(t) = g_L v(t) + I_L(t-\Delta t) \tag{2.9}$$

$$g_L = (\frac{\Delta t}{2L}) \tag{2.10}$$

$$I_L(t-\Delta t) = i(t-\Delta t) + g_L v(t-\Delta t) \tag{2.11}$$

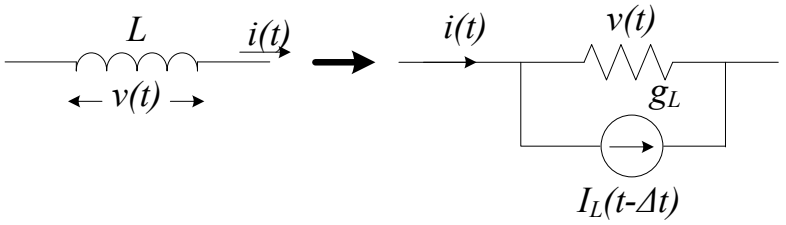

FIGURE 2.3: The Norton's equivalent of an inductor

Modelling a Capacitor using Dommel's Algorithm

Equation (2.15) represents the Norton equivalent model, which can be derived by applying the trapezoidal rule of integration to (2.12). Here $I_C(t-\Delta t)$ is the history term, which can be regarded as the current source of the Norton equivalent. The term g_C can be regarded as the conductance parallel with the current source. The

Norton equivalent circuit of the capacitor is shown in the Figure 2.4.

$$i = C\frac{d}{dt}v \tag{2.12}$$

$$v(t) = v(t-\Delta t) + \frac{\Delta t}{2C}\Big[i(t-\Delta t) + i(t)\Big] \tag{2.13}$$

$$i(t) = \frac{2C}{\Delta t}v(t) - \frac{2C}{\Delta t}v(t-\Delta t) - i(t-\Delta t) \tag{2.14}$$

$$i(t) = g_C v(t) + I_C(t-\Delta t) \tag{2.15}$$

$$g_C = (\frac{2C}{\Delta t}) \tag{2.16}$$

$$I_C(t-\Delta t) = -g_C v(t-\Delta t) - i(t-\Delta t) \tag{2.17}$$

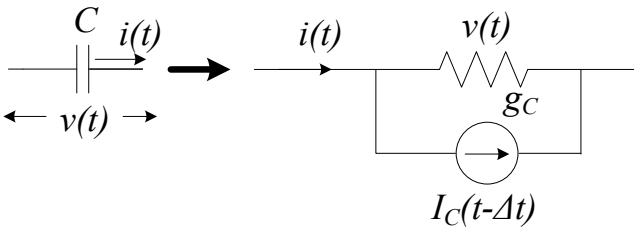

FIGURE 2.4: The Norton's equivalent of a capacitor

2.1.2 Real-Time Digital Simulator (RTDS)

RTDS is a real time implementation of Dommel's EMT algorithm. Real time simulation of the power system is useful to study the interactions of the equipment like protective relays, power electronic devices (e.g., FACTS), control devices and etc. Real time simulation of electromagnetic transients are done by dividing the power system into sub systems and solving each of these networks in parallel using a separate processor. In order to do this the travelling time of the transmission line connecting the two sub systems should be greater than the time step of the simulation [12]. RTDS adopts this concept to provide the user the capability of simulating any size of a power system, by dividing it into sub systems. The each of the subsystems can be modelled in a separate RTDS rack. As the size of the simulation network increases, the number of processors required will increase.

RTDS simulation software is named RSCAD, which gives user a platform to make a draft, compile and run it in a separate window (the run time window). The component library of RSCAD contains a large number of pre-defined components. Apart from that, RTDS gives users the capability of building their own components in the interface named C-Builder. The user can write their own C-code to design a power system or a control system component. It also allows the user to draw their own symbols for the component.

As mentioned earlier to simulate a large power system, higher number of racks are needed. One rack of RTDS can model maximum of 30 three phase buses using the fibre enhanced backplane [13] (without the fibre enhanced backplane the limit is 24 three-phase buses). Therefore, RTDS requires large number of powerful processing units to analyse large power systems.

2.2 Dynamic Phasor Equivalent

In dynamic phasor modelling a three phase signal is represented using its magnitude and angle which are allowed to change over time. In transient stability type simulations the derivative of the currents and voltages are replaced by "$j\omega$"(where ω is the angular frequency) so the power transfer will only happens at the system frequency. But in dynamic phasors the differential equations are solved using numerical integration methods. Therefore, dynamic phasor models are capable of modelling some of the electromagnetic transients (e.g., power electronic devices like FACTS, TCSC and etc.) involved in the power system [14]. In dynamic phasors the oscillatory part (ωt) of the phasor signal is removed by multiplying the signal by $e^{-j\omega t}$ resulting in constant phasors in steady state [15]. Consider a constant rotating AC voltage (v_{ac}) and current (i_{ac}) with a phase difference of θ in (2.18) and (2.19) [16] where ϕ is the angle of the voltage signal. The terms V_m and I_m are the magnitudes of the voltage and current signals.

$$v_{ac} = V_m e^{j\phi} e^{j\omega t} = [V_R + jV_I] e^{j\omega t} \tag{2.18}$$

$$i_{ac} = I_m e^{j(\phi+\theta)} e^{j\omega t} = [I_R + jI_I] e^{j\omega t} \tag{2.19}$$

where ,

$$V_R = V_m \cos(\phi) \qquad V_I = V_m \sin(\phi) \tag{2.20}$$

$$I_R = I_m \cos(\phi + \theta) \qquad I_I = I_m \sin(\phi + \theta) \tag{2.21}$$

The terms V_R and V_I denote the real and the imaginary part of the voltage v_{ac} and the terms I_R and I_I denote the real and the imaginary part of the current i_{ac}.

Dynamic phasor models are accurate only when the system frequency of the simulation does not change significantly over time. In this study, dynamic

phasors are used only to study balanced, harmonic free three-phase systems. This topic will be discussed at greater length in Chapter 3.

2.3 Hybrid Simulation of Electromagnetic Transient Model and Dynamic Phasor Equivalent

As discussed in the previous chapter designing the FDNE of the external system for the TSA-EMT hybrid simulation is a difficult task. Moreover it degrades the accuracy of the whole simulation model. Hence, the researchers are trying to come up with an alternative method which would replace/modify the FDNE in the hybrid simulation. Interfacing the dynamic phasor type simulation to the EMT model promises several advantages compared to EMT-TSP hybrid simulation. The dynamic phasor model covers higher bandwidth compared to TSP model therefore the external system would be modelled in more details compared to TSP. Since the dynamic phasor equivalent and the EMT model share similar characteristics, there will be no need of an FDNE filter at the interface to represent fast high frequency transients of the external system.

Since the dynamic phasor equivalent can be modelled using higher time step and also using only two phasors instead of three, the dynamic phasor-EMT hybrid simulation will reduce the computational burden significantly compared to EMT simulation. In this research the crucial part of the network (internal system) containing power electronic devices and switches are modelled using the EMT type simulation and the less important part of the network (external system) is modelled using the dynamic phasor equivalent (Figure 2.5).

This concept can be later apply to the TSP-EMT hybrid simulation to

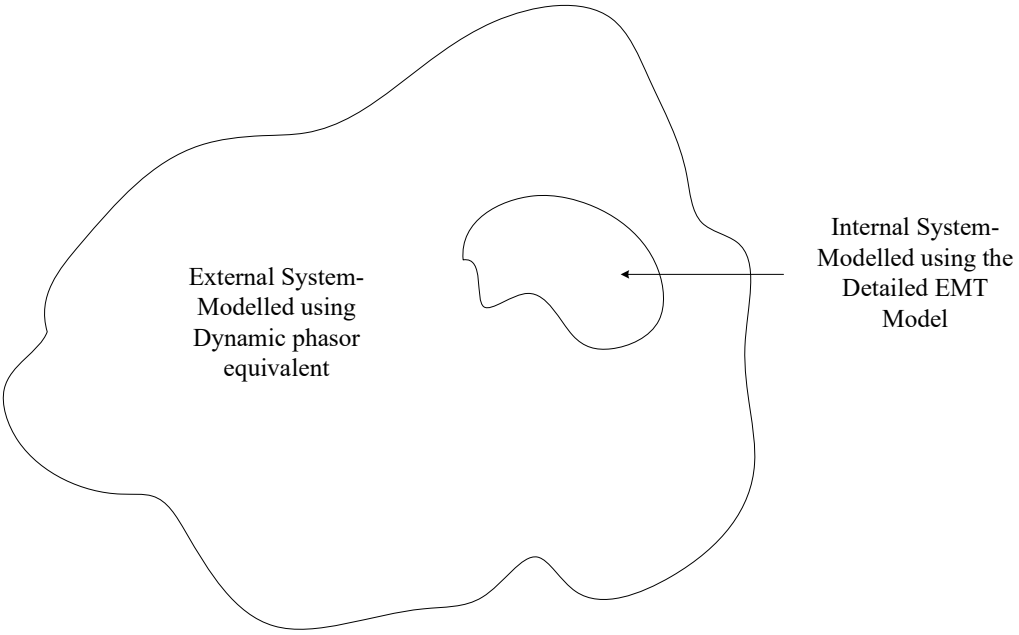

FIGURE 2.5: The internal and the external system of the hybrid simulation

replace the FDNE model. Dynamic phasors can be used to simulate the network between the EMT-TSP model including the interfacing nodes. Since TSP and dynamic phasors are both phasor domain simulations the interfacing these two models would be easier. This method can be used to simulate large power systems.

2.3.1 Representing External System Equivalent in the Electromagnetic Transient Simulation

In electromagnetic transient type simulation all the power system components are modelled as a Norton equivalent and the system is solved using nodal analysis. When a part of the network is modelled using dynamic phasor equivalent, depending on the network topology there can be one or more nodes in the network at the interface between the EMT model and the dynamic phasor equivalent. The EMT

model sees the external system as a current source in parallel with a conductor at each of these nodes. The value of the current source and the conductor is derived in every time step at the dynamic phasor equivalent.

2.3.2 Representing Internal System Equivalent in the Dynamic Phasor Model

In the dynamic phasor model, the EMT model is represented as a voltage source at each of the interfacing point. The dynamic phasor program reads the voltages of the interfacing nodes and it injects current back to the EMT model in every time step (Figure 2.6).

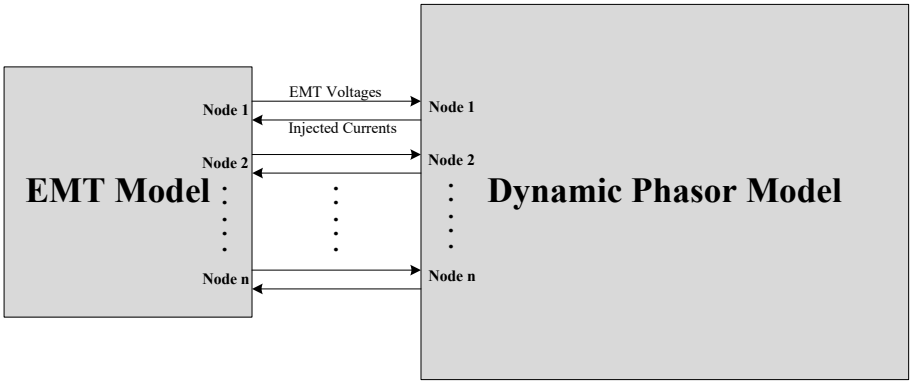

FIGURE 2.6: Interfacing the dynamic phasor equivalent to the EMT model

Chapter 3

Dynamic Phasor Models for Time Domain Simulation

3.1 Introduction

In this chapter modelling a simple power system using dynamic phasors is described. To model a power system using dynamic phasors, all the components (generators, machines, loads, transmission lines etc.) have to be modelled using dynamic phasors. As this research is mainly focused on interfacing dynamic phasors to the EMT simulation, only some of the basic components in a power system are modelled using dynamic phasors.

Most of the power system components can be represented using RL and RC circuits [16]. As an example, a transmission line can be modelled using its PI section model so that it will contain only series RL and shunt RC branches. The five bus network in Figure 3.1, which has four transmission lines and a load is represented using PI section model and used as the simulation case for this study.

In this network, nodes 1, 2 and 3 are are connected to the EMT model and are considered as interfacing buses between the EMT model and the dynamic phasor model. The nodes 4 and 5 are inside the dynamic phasor model and are modelled as dynamic phasor nodes. The resulting "$\frac{C}{2}$" capacitors of the PI section model derived from the transmission lines connected to the interfacing nodes are not modelled in dynamic phasors and will be discussed in Chapter 6. In this study the

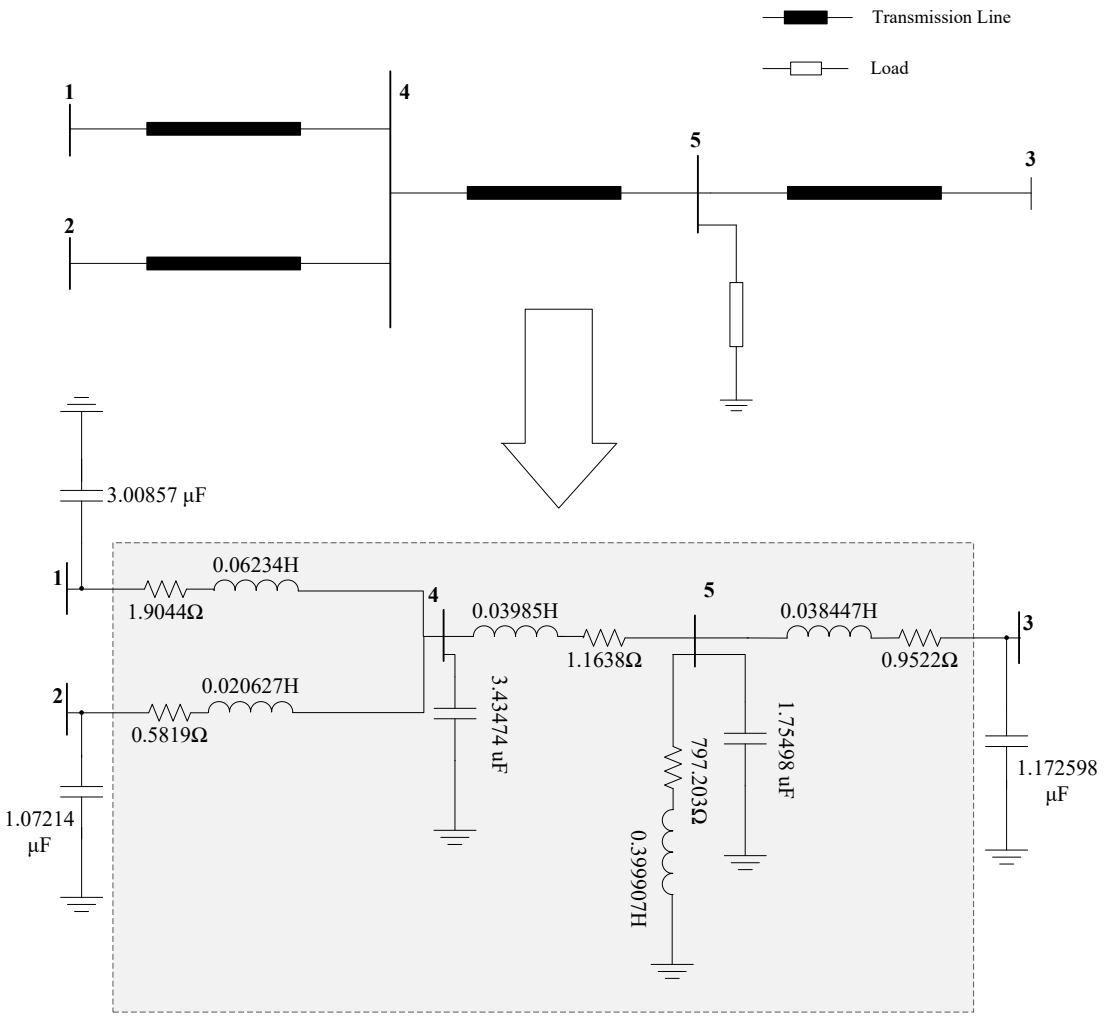

FIGURE 3.1: The simulation network modelled using RL and RC branches

network in Figure 3.1 is modelled using state space representation (Section 3.2)[16].

An alternative method, which is similar to nodal analysis discussed in Chapter 2 is also used to model the network in Figure 3.1. Moreover the performance of the two methods is discussed.

3.2 Method 1: State Space Modelling

3.2.1 Dynamic Phasor Representation of the Power System

In this section, series RL and a shunt RC branch will be modelled in dynamic phasors using state space models. The dynamic phasor equations for each component is derived and numerical integration methods for solving the state equations are discussed. Finally a solution for the network in Figure 3.1 is derived.

Dynamic Phasor Representation of a Series RL Branch

Consider the series RL component connected between node 1 and node 4 in Figure 3.1, where node 1 is an interface bus. The voltage drop across the series RL branch can be expressed as,

$$v_{14} = L\frac{di}{dt} + Ri \tag{3.1}$$

Taking,

$$v_{14} = V_m * e^{jwt} \quad and \quad i = I_m * e^{jwt} * e^{j\theta} \tag{3.2}$$

and by removing the rotational part it can be shown that,

$$\tilde{V}_{14} = (R + jw_0L)\tilde{I} + \frac{Ld\tilde{I}}{dt} \tag{3.3}$$

where, $\tilde{V}$ and $\tilde{I}$ are the phasor values of voltages and currents. By separating the real and imaginary parts of (3.3),

$$\frac{\mathrm{d}}{\mathrm{d}t}\begin{bmatrix} I_R \\ I_I \end{bmatrix} = \begin{bmatrix} -R/L & w_0 & -1/L & 0 \\ -w_0 & -R/L & 0 & -1/L \end{bmatrix} \begin{bmatrix} I_R \\ I_I \\ V_{4R} \\ V_{4I} \end{bmatrix} + \frac{1}{L}\begin{bmatrix} V_{1R} \\ V_{1I} \end{bmatrix} \tag{3.4}$$

The resulting model is a state space model where X is the state vector.

$$\dot{X} = AX + BU \tag{3.5}$$

where,

$$A = \begin{bmatrix} -R/L & w_0 & -1/L & 0 \\ -w_0 & -R/L & 0 & -1/L \end{bmatrix} \quad B = \frac{1}{L} \tag{3.6}$$

The input vector U is the real and imaginary parts of the voltage at node 1.

$$U = \begin{bmatrix} V_{1R} \\ V_{1I} \end{bmatrix} \tag{3.7}$$

The state vector X contains the state variables I_R and I_I associated with the RL branch and V_{4R} and V_{4I} associated with the node 4 voltage described in the next topic. All the RL baranches in the network can be modelled in a similar way and the corresponding state equations can be derived.

Dynamic Phasor Representation of a Parallel RC Branch

Consider the shunt RC branch connected to the node 4,

$$i = C\frac{dv}{dt} + \frac{1}{R}v \tag{3.8}$$

$$\tilde{I} = (G + jw_0C)\tilde{V_4} + C\frac{d\tilde{V_4}}{dt} \tag{3.9}$$

By separating the real and imaginary parts of the equation,

$$\frac{\mathrm{d}}{\mathrm{d}t}\begin{bmatrix} V_{4R} \\ V_{4I} \end{bmatrix} = \begin{bmatrix} -G/C & w_0 \\ -w_0 & -G/C \end{bmatrix}\begin{bmatrix} V_{4R} \\ V_{4I} \end{bmatrix} + \frac{1}{C}\begin{bmatrix} I_R \\ I_I \end{bmatrix} \tag{3.10}$$

The resulting model is a state space model where, state variables are the real and the imaginary values of the voltage at node 4.

$$\dot{X} = AX + BU \tag{3.11}$$

Where,

$$A = \begin{bmatrix} -G/C & w_0 \\ -w_0 & -G/C \end{bmatrix} \quad B = \frac{1}{C} \tag{3.12}$$

and input vector U is the real and imaginary parts of the currents into the node 4.

$$U = \begin{bmatrix} I_R \\ I_I \end{bmatrix} \tag{3.13}$$

All the states of the network in the Figure 3.3 can be derived using these equations. For this network the state variables will be the real and the imaginary parts of the currents in RL branches and the voltages of the shunt capacitors. The inputs of the state equations will be the EMT node voltages at node 1,2 and 3.

3.2.2 Numerical Integration

The state equations are solved by numerically integrating it in each time step in digital time domain simulation. The size of the integration time step is important for accurate and stable results. The state equation can be numerically integrated using numerous methods. In EMT type simulation, the trapezoidal rule of integration is used since it is stability preserving. The fourth order Runge-Kutte is also a popular method of integration. The trapezoidal rule of integration is used to solve the differential equations in this research for the interface between the EMT model and the dynamic phasor model to be smoother.

The state space equation can be solved using the trapezoidal rule of integration as follows.

$$X_{n+1} = X_n + \frac{1}{2}\big(AX_n + BU_n + AX_{n+1} + BU_{n+1}\big)\Delta t \tag{3.14}$$

$$X_{n+1} = \big(I - \frac{\Delta t}{2}A\big)^{-1}\big(I + \frac{\Delta t}{2}A\big)X_n + \big(I - \frac{\Delta t}{2}A\big)^{-1}BU \tag{3.15}$$

The complete flow chart containing all the computational steps of Method 1 (state space modelling) is shown in Figure 3.2 .

3.3 Method 2: Nodal Analysis

In this section, the network components are modelled in a way that is similar to the nodal analysis in EMTP. All the components in Figure 3.1 is modelled using it's Norton equivalent circuit and the network equation is solved using Kirchoff's current law.

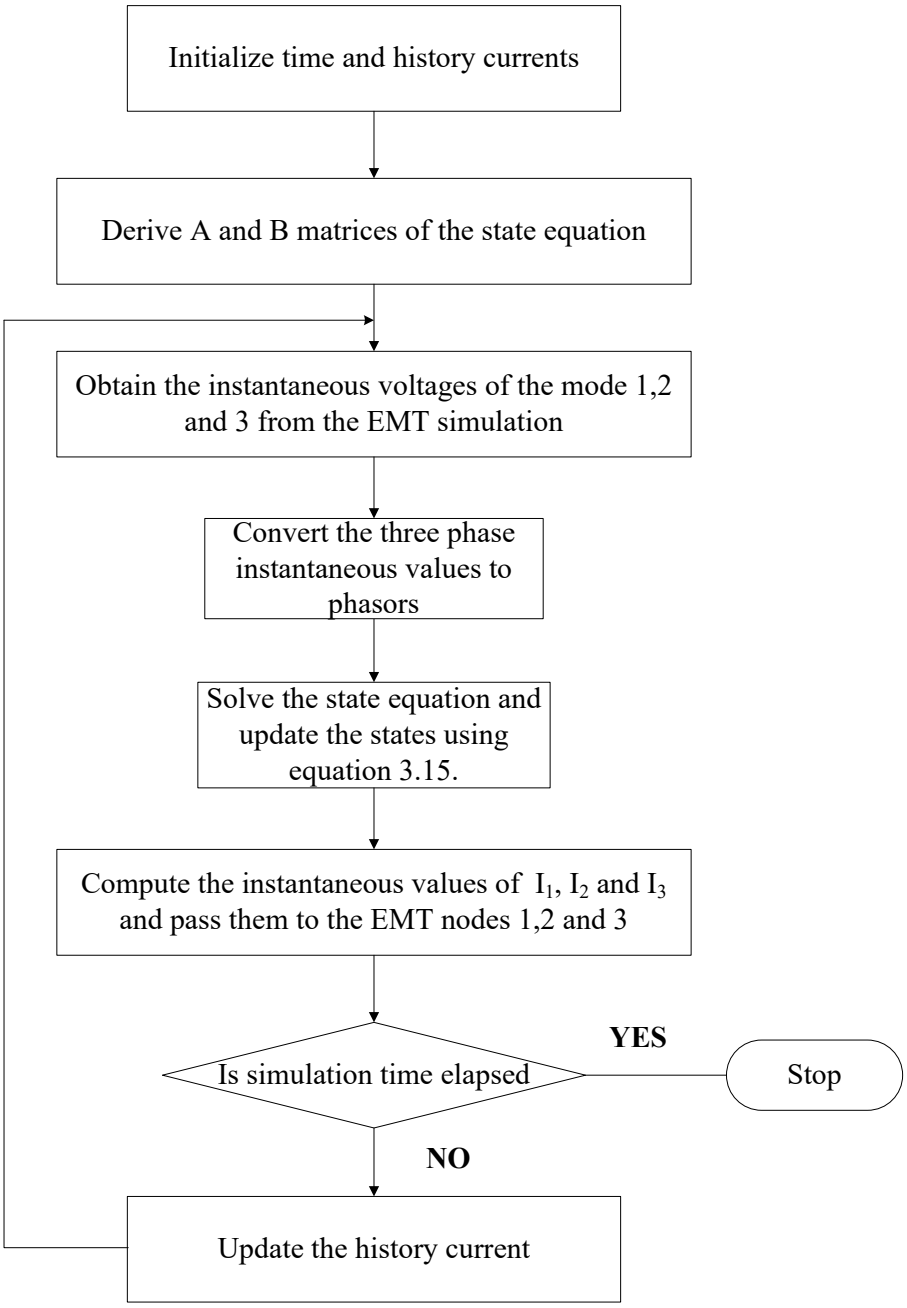

FIGURE 3.2: The computational steps involved with the state space modelling using dynamic phasors

Dynamic Phasor Representation of a RL Branch

The equation for a RL branch in dynamic phasors can be derived using (3.1) and (3.2).

$$\tilde{V}_{12} = L\frac{d}{dt}\tilde{I} + (R + j\omega_0 L)\tilde{I} \tag{3.16}$$

$$\frac{d}{dt}\tilde{I} = -(\frac{R}{L} + j\omega_0)\tilde{I} + \frac{1}{L}\tilde{V}_{12} \tag{3.17}$$

By applying trapezoidal rule of integration,

$$\begin{aligned} I(t) = I(t-1) + \Bigg[&- \big(\frac{R}{L} + j\omega_0\big)I(t-1) + \frac{1}{L}\tilde{V}_{12}(t-1) \\ &- \big(\frac{R}{L} + j\omega_0\big)I(t) + \frac{1}{L}\tilde{V}_{12}(t)\Bigg]\frac{\Delta t}{2} \end{aligned} \tag{3.18}$$

Rearranging (3.18),

$$\begin{aligned} \left[1 + \frac{R\Delta t}{2L} + j\frac{\omega_0\Delta t}{2}\right]I(t) = &\left[1 - \frac{R\Delta t}{2L} + j\frac{\omega_0\Delta t}{2}\right]I(t-1) + \\ &\frac{\Delta t}{2L}\tilde{V}_{12}(t-1) + \frac{\Delta t}{2L}\tilde{V}_{12}(t) \end{aligned} \tag{3.19}$$

$$\tilde{I}(t) = \tilde{h}_1\tilde{V}_{12}(t-1) + \tilde{h}_2\tilde{I}_{12}(t-1) + \tilde{Y}\tilde{V}_{12}(t) \tag{3.20}$$

Where,

$$\tilde{h_2} = \frac{1 - \frac{R\Delta t}{2L} - j\frac{\omega_0\Delta t}{2}}{1 + \frac{R\Delta t}{2L} + j\frac{\omega_0\Delta t}{2}} \tag{3.21}$$

$$\tilde{h_1} = \tilde{Y} = \frac{\frac{\Delta t}{2L}}{1 + \frac{R\Delta t}{2L} + j\frac{\omega_0\Delta t}{2}} \tag{3.22}$$

The circuit model for the series RL branch is in Figure 3.3, where I_H denotes the history term which is expressed in (3.23).

$$I_H = \tilde{h}_1\tilde{V}_{12}(t-1) + \tilde{h}_2\tilde{I}_{12}(t-1) \tag{3.23}$$

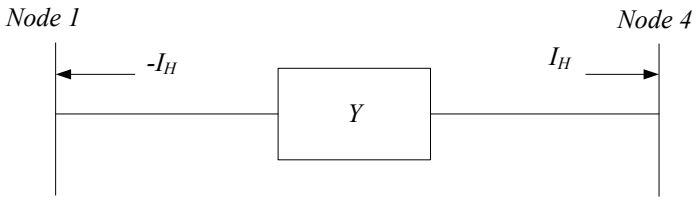

FIGURE 3.3: The circuit model for a series RL branch

Dynamic Phasor Representation of a Parallel RC Branch

The equation for a RC branch in dynamic phasors can be derived using (3.8) and (3.9).

$$\tilde{I} = C\frac{d}{dt}\tilde{V} + (G + j\omega_0 C)\tilde{V} \tag{3.24}$$

$$\frac{d}{dt}\tilde{V} = -(\frac{G}{C} + j\omega_0)\tilde{V} + \frac{1}{C}\tilde{I} \tag{3.25}$$

By applying trapezoidal rule of integration,

$$\begin{aligned}\tilde{V}(t) = \tilde{V}(t-1) + \Bigg[&- (\frac{G}{C} + j\omega_0)\tilde{V}(t-1) + \frac{1}{C}\tilde{I}(t-1) + \\ &(\frac{G}{C} + j\omega_0)\tilde{V}(t) + \frac{1}{C}\tilde{I}(t)\Bigg]\frac{\Delta t}{2}\end{aligned} \tag{3.26}$$

$$\begin{aligned}\frac{\Delta t}{2C}\tilde{I}(t) = -\frac{\Delta t}{2C}\tilde{I}(t-1) - &\left[1 - \frac{G\Delta t}{2C} - j\frac{\omega_0 \Delta t}{2}\right]\tilde{V}(t-1) + \\ &\left[1 + \frac{G\Delta t}{2C} + j\frac{\omega_0 \Delta t}{2}\right]\tilde{V}(t)\end{aligned} \tag{3.27}$$

$$\tilde{I}(t) = \tilde{h}_1\tilde{V}(t-1) + \tilde{h}_2\tilde{I}(t-1) + \tilde{Y}\tilde{V}(t) \tag{3.28}$$

Where,

$$\tilde{h}_2 = -1 \tag{3.29}$$

$$\tilde{h}_1 = -\frac{1 - \frac{G\Delta t}{2C} - j\frac{\omega_0 \Delta t}{2}}{\frac{\Delta t}{2C}} \tag{3.30}$$

$$\tilde{Y} = \frac{1 + \frac{G\Delta t}{2C} + j\frac{\omega_0 \Delta t}{2}}{\frac{\Delta t}{2C}} \tag{3.31}$$

The circuit model for a shunt RC branch is in Figure 3.4, where I_H denotes the history term which is expressed in (3.32).

$$I_H = \tilde{h}_1 \tilde{V}(t-1) + \tilde{h}_2 \tilde{I}(t-1) \tag{3.32}$$

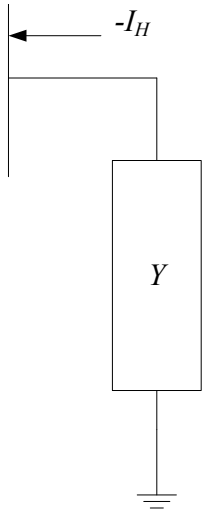

FIGURE 3.4: The circuit model for a shunt RC branch

All the components in the Figure 3.1 can now be represented as a current source in parallel with a conductance (Figure 3.5). The components of the admittance matrix and the history currents going out from the nodes can be calculated from the Figure 3.5. Then the network can be solved using Kirchoff's current law and the new voltages can be derived similar to the EMT simulation.

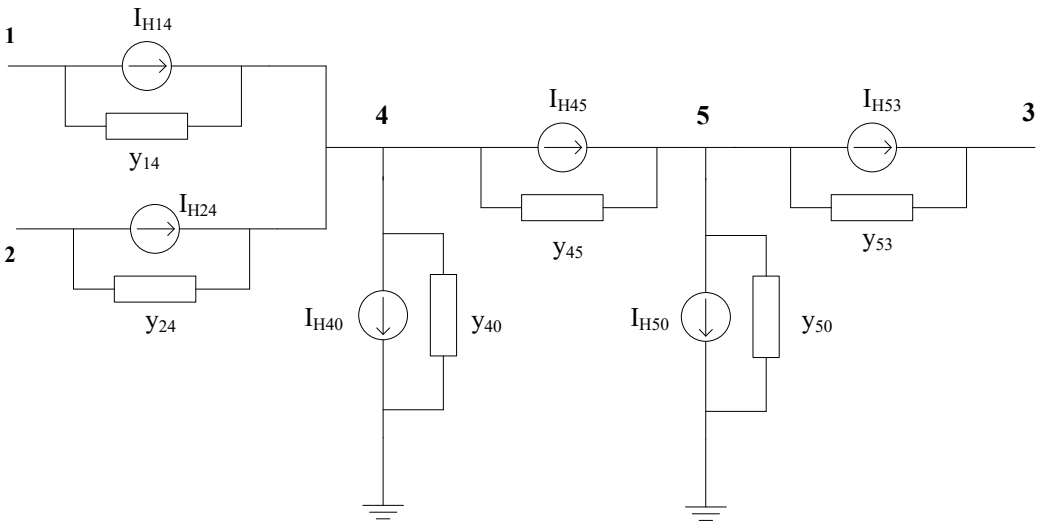

FIGURE 3.5: The simulation case represented using the Norton equivalent circuits

$$\begin{bmatrix} I_1 \\ I_2 \\ I_3 \\ I_4 \\ I_5 \end{bmatrix} = \begin{bmatrix} Y_{11} & Y_{12} & Y_{13} & Y_{14} & Y_{15} \\ Y_{21} & Y_{22} & Y_{23} & Y_{24} & Y_{25} \\ Y_{31} & Y_{32} & Y_{33} & Y_{34} & Y_{35} \\ Y_{41} & Y_{42} & Y_{43} & Y_{44} & Y_{45} \\ Y_{51} & Y_{52} & Y_{53} & Y_{54} & Y_{55} \end{bmatrix} \begin{bmatrix} V_1 \\ V_2 \\ V_3 \\ V_4 \\ V_5 \end{bmatrix} + \begin{bmatrix} I_{h1} \\ I_{h2} \\ I_{h3} \\ I_{h4} \\ I_{h5} \end{bmatrix} \tag{3.33}$$

$$\begin{bmatrix} I_1 \\ I_2 \\ I_3 \end{bmatrix} = \begin{bmatrix} Y_{11} & Y_{12} & Y_{13} & Y_{14} & Y_{15} \\ Y_{21} & Y_{22} & Y_{23} & Y_{24} & Y_{25} \\ Y_{31} & Y_{32} & Y_{33} & Y_{34} & Y_{35} \end{bmatrix} \begin{bmatrix} V_1 \\ V_2 \\ V_3 \\ V_4 \\ V_5 \end{bmatrix} + \begin{bmatrix} I_{h1} \\ I_{h2} \\ I_{h3} \end{bmatrix} \tag{3.34}$$

$$\begin{bmatrix} 0 \\ 0 \end{bmatrix} = \begin{bmatrix} Y_{41} & Y_{42} & Y_{43} & Y_{44} & Y_{45} \\ Y_{51} & Y_{52} & Y_{53} & Y_{54} & Y_{55} \end{bmatrix} \begin{bmatrix} V_1 \\ V_2 \\ V_3 \\ V_4 \\ V_5 \end{bmatrix} + \begin{bmatrix} I_{h4} \\ I_{h5} \end{bmatrix} \tag{3.35}$$

$$\begin{bmatrix} V_4 \\ V_5 \end{bmatrix} = - \begin{bmatrix} Y_{44} & Y_{45} \\ Y_{54} & Y_{55} \end{bmatrix}^{-1} \begin{bmatrix} Y_{41} & Y_{42} & Y_{43} \\ Y_{51} & Y_{52} & Y_{53} \end{bmatrix} \begin{bmatrix} V_1 \\ V_2 \\ V_3 \end{bmatrix} - \begin{bmatrix} Y_{44} & Y_{45} \\ Y_{54} & Y_{55} \end{bmatrix}^{-1} \begin{bmatrix} I_{h4} \\ I_{h5} \end{bmatrix} \tag{3.36}$$

The complete flow chart containing all the computational steps is in Figure 3.6.

The conversion between three phase instantaneous values and its phasor values has to be done in back and fourth in each iteration. The phasor currents are converted to their instantaneous values using equations 3.37, 3.38 and 3.39 assuming three phase balanced conditions. Here I_m is the magnitude of the phasor current and the θ is the angle.

$$I_a = I_m \sin(\omega_0 t + \theta) \tag{3.37}$$

$$I_b = I_m \sin(\omega_0 t - \frac{2\pi}{3} + \theta) \tag{3.38}$$

$$I_c = I_m \sin(\omega_0 t + \frac{2\pi}{3} + \theta) \tag{3.39}$$

The conversion of the three phase instantaneous values of voltages to its phasor domain will be discussed in the next chapter.

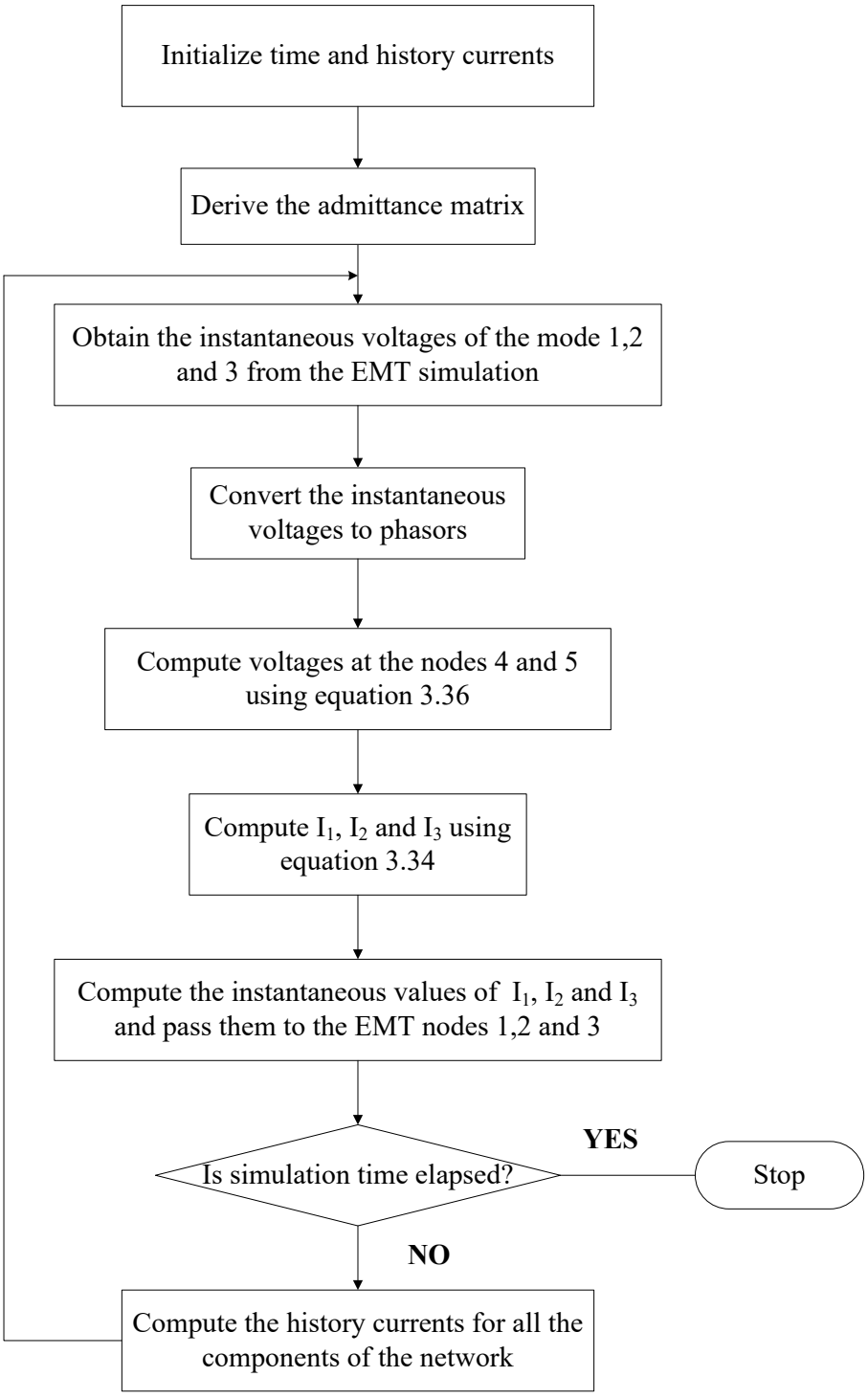

FIGURE 3.6: The computational steps involved with the nodal analysis using dynamic phasors

Chapter 4

Interfacing Dynamic Phasor Solution to an Electromagnetic Transient Type Simulation

Electromagnetic transient-type simulations are done using time domain instantaneous values of voltages and currents. Since the dynamic phasor model uses phasor values of voltages and currents, there should be a method to interface these different types of solutions. In TSA to EMT type hybrid simulation this conversion is done using energy balance [4], a fast Fourier transformation (FFT) [17] or a consecutive curve fitting technique [18].

Phase locked loops (PLL) are widely used for determining the phase angle and the magnitude of the three phase grid voltage. The real and imaginary parts of three phase instantaneous voltages can be calculated by connecting a PLL to the interface between the EMT model and the dynamic phasor equivalent. Using the phasor values of the EMT node voltages, the phasor type network solution can be derived and sent to the EMT model as an injected current. In this research a

synchronous reference frame PLL is used for phasor conversion since it has better performance compared to other PLL structures under non ideal grid conditions [19]. The basic structure of the SRF-PLL is described in Section 4.1.2.

4.1 Phase Locked Loop

4.1.1 PLL synchronization

The basic structure of a PLL is shown in Figure 4.1 which has three fundamental blocks named "Phase Detector", "Loop Filter" and "Voltage Controlled Oscillator". The phase detector block generates a signal proportional to the phase difference between the two input signals. The loop filter contains a PI controller and/or a low pass filter which removes the high frequency components of the input signal and VCO outputs a signal that follows the input [20].

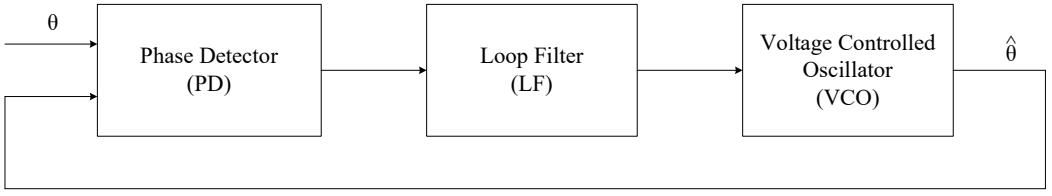

FIGURE 4.1: The basic structure of a PLL

4.1.2 Synchronous Reference Frame PLL

The SRF-PLL is the most widely used PLL type to estimate the angle in a three phase signal. The structure of the SRF-PLL is simple yet fast and accurate. The

functional block diagram of the SRF PLL is shown in the Figure 4.2 [21]. When positive sequence three phase instantaneous voltages are given as the input to the SRF-PLL, the control system is capable of estimating the phase angle (θ) of the phase "a" signal.

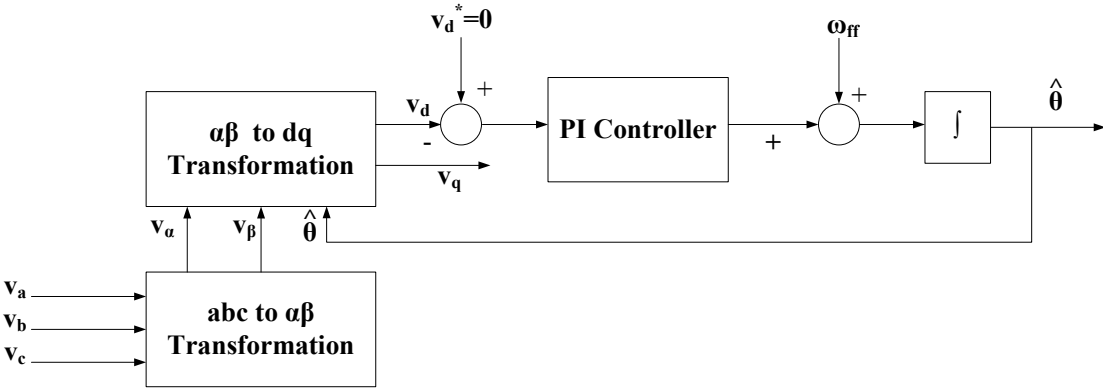

FIGURE 4.2: The basic structure of the SRF-PLL

To track the phase angle, three phase voltages are transformed to a stationary system of two phases V_d and V_q . Assuming balanced conditions, a three phase voltage vector can be converted into their alpha-beta components using Clarke transformation as shown in (4.1) - (4.6).

$$v_a = V_m \sin\theta \tag{4.1}$$

$$v_b = V_m \sin\left(\theta - \frac{2\pi}{3}\right) \tag{4.2}$$

$$v_c = V_m \sin\left(\theta + \frac{2\pi}{3}\right) \tag{4.3}$$

$$T_{\alpha\beta} = \begin{bmatrix} 1 & -\frac{1}{2} & -\frac{1}{2} \\ 0 & -\frac{\sqrt{3}}{2} & \frac{\sqrt{3}}{2} \end{bmatrix} \tag{4.4}$$

$$v_{abc} = \begin{bmatrix} v_a & v_b & v_c \end{bmatrix}^{\mathsf{T}} \tag{4.5}$$

$$v_{\alpha\beta} = T_{\alpha\beta} * v_{abc} \tag{4.6}$$

$$\begin{bmatrix} v_\alpha \\ v_\beta \end{bmatrix} = \begin{bmatrix} V_m \sin\theta \\ V_m \cos\theta \end{bmatrix} \tag{4.7}$$

Note that θ is not required to compute v_α and v_β using (4.6) although they can be expressed in terms of θ as shown in (4.7).

The phase angle θ is tracked by aligning the voltage vector along the q axis. The q-axis transformation matrix is,

$$T_{qd} = \begin{bmatrix} \sin\hat{\theta} & \cos\hat{\theta} \\ \cos\hat{\theta} & -\sin\hat{\theta} \end{bmatrix} \tag{4.8}$$

where $\hat{\theta}$ is the estimated phase angle output of the PLL. The alpha-beta components of the voltages are then converted to the dq coordination system using (4.9).

$$v_{qd} = T_{qd} * v_{\alpha\beta} \tag{4.9}$$

$$v_{qd} = \begin{bmatrix} V_m \cos(\theta - \hat{\theta}) \\ -V_m \sin(\theta - \hat{\theta}) \end{bmatrix} \tag{4.10}$$

Aligning the voltage vector along the q axis will results the d axis voltage (v_d) to become zero. Now if $\hat{\theta} \approx \theta$ in (4.10), the term v_d will equal to zero. Therefore, the gains of the PI-regulator is tuned so that v_d follows the reference value $v_d^\star = 0$. This will yield the estimated phase angle ($\hat{\theta}$) to be equal to phase angle θ. In this condition, v_q will be equal to the amplitude of the input voltage. The phasor values are obtained as,

$$V_{Real} = v_q * \cos\theta, \quad V_{Imaginary} = v_q * \sin\theta \tag{4.11}$$

4.2 Simulation Procedure and Results

The network in Figure 3.1 was modelled in MATLAB using dynamic phasor models described in Section 3.2 and Section 3.3. Three phase balanced instantaneous voltages were generated as the EMT node voltages. The SRF-PLL in Section 4.1.2 was connected to the interface to convert the three phase instantaneous values to its phasor domain. Each interface bus was connected to a PLL. The results of the two dynamic phasor models were compared with a PSCAD EMT model. This was done by implementing the Figure 3.1 network in PSCAD and connecting three voltage sources containing the same voltages that were given to the dynamic phasor model. Initially the time step of 50μs was used as the simulation time step. Then the time step was increased until the dynamic phasor equivalent results started to deviate from the EMT-PSCAD results. A step voltage disturbance was injected to the input at 0.1s. The voltages of the interface nodes before and after the disturbance is shown in the table 4.1.

TABLE 4.1: Voltages of the Interface Nodes Before and After the Disturbance

	Before		After	
Node	Voltage /kV	Phase angle /rad	Voltage /kV	Phase angle /rad
1	230.00	0	239.20	0
2	232.30	0	232.30	0
3	231.84	0	234.61	0.567

4.2.1 Simulation Results of the State Space Model

Figure 4.3, 4.4 and 4.5 show the injected currents to the EMT nodes when the network in Figure 3.1 was simulated using state space analysis in dynamic phasors using a time step of 50μs. The results are compared with the results from the

EMT model. Considering the results, it can be said that the resultant dynamic phasor model gives similar results as the EMT simulation. The same simulation was carried out using a time step of 500μs and the results are shown in Figure 4.6, 4.7 and 4.8.

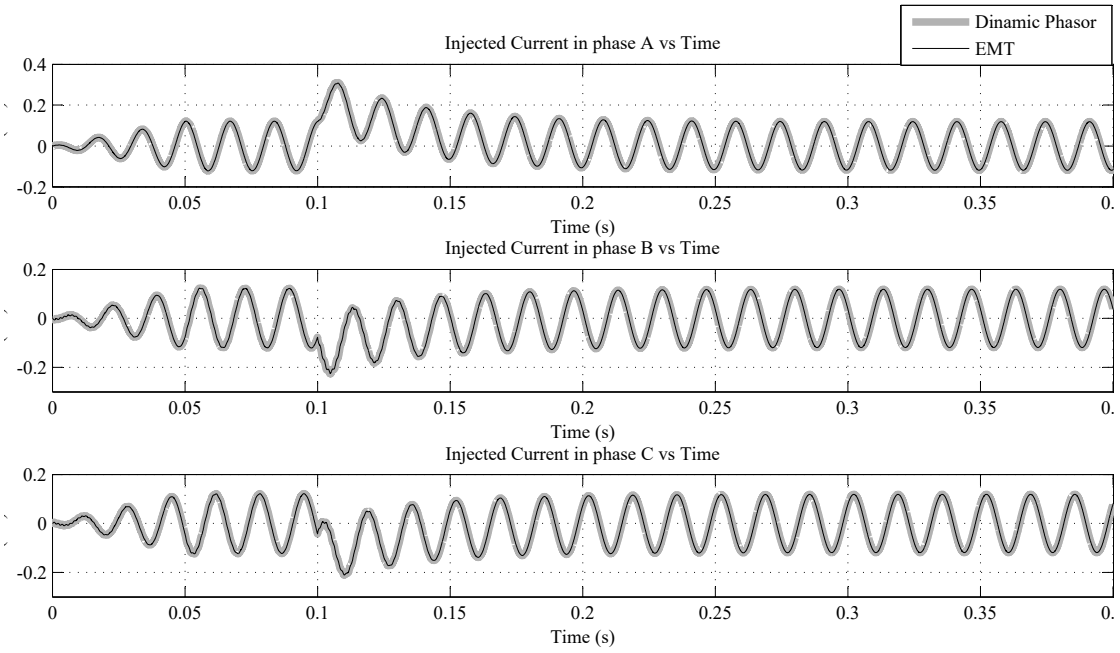

FIGURE 4.3: The injected currents to the node 1 with the time step of 50μs

4.2.2 Simulation Results of Nodal Analysis

Figure 4.9, 4.10 and 4.11 show the injected currents to the EMT nodes when Figure 3.1 was simulated using the nodal analysis in dynamic phasors. Considering the comparison of the results with the EMT model it can be said that the resultant model adequately represents the network.

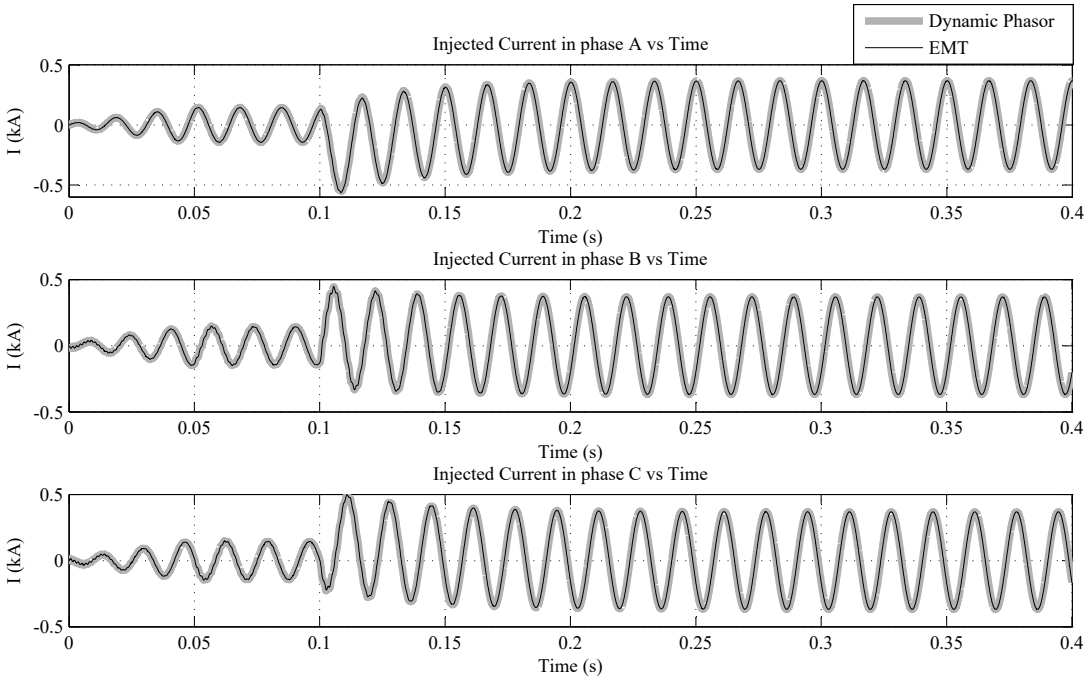

FIGURE 4.4: The injected currents to the node 2 with the time step of 50μs

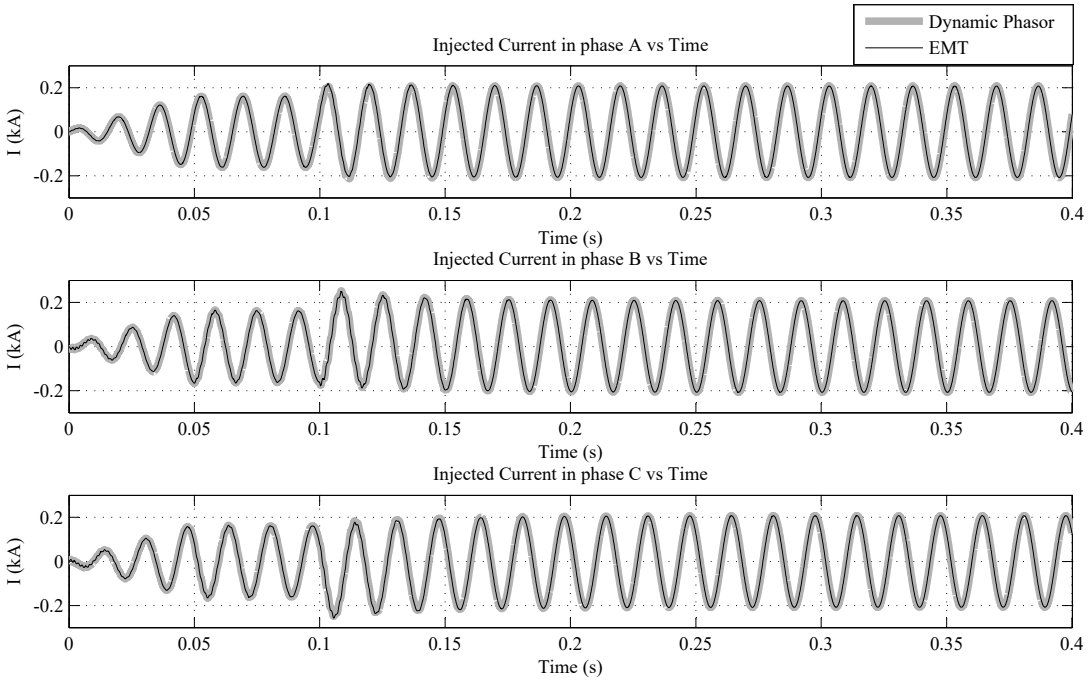

FIGURE 4.5: The injected currents to the node 3 with the time step of 50μs

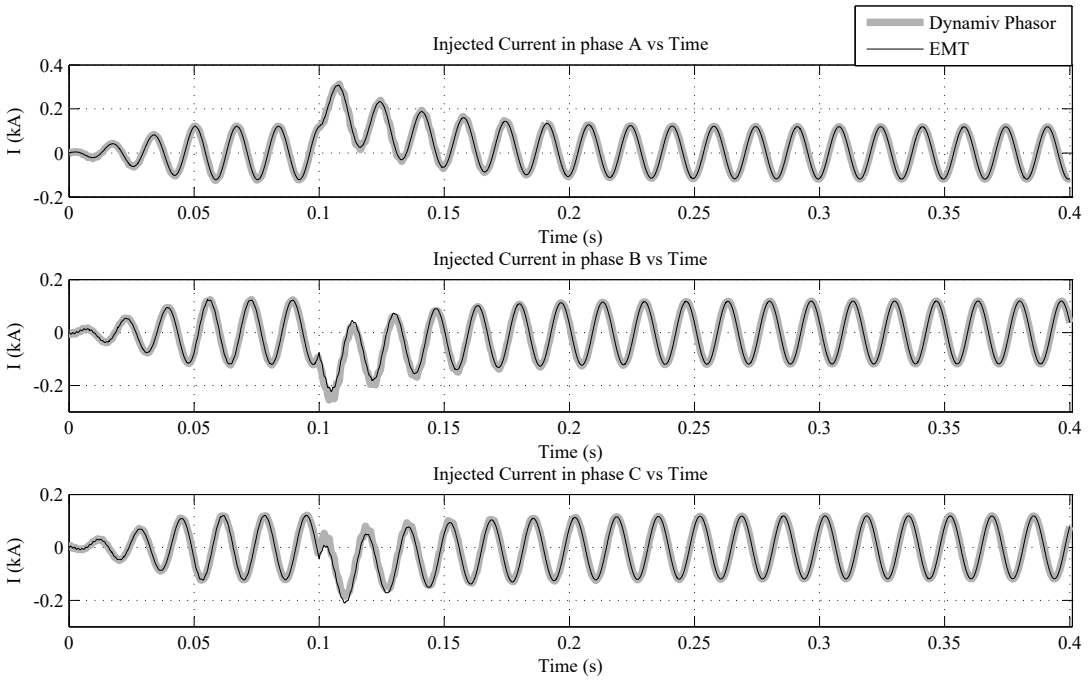

FIGURE 4.6: The injected currents to the node 1 with the time step of 500μs

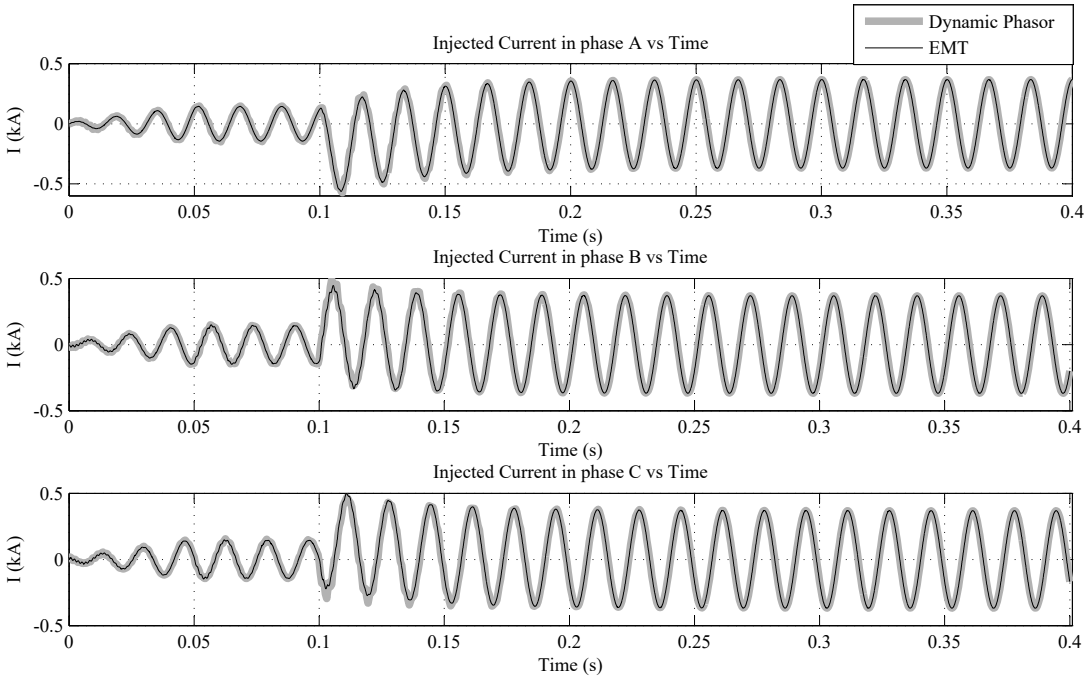

FIGURE 4.7: The injected currents to the node 2 with the time step of 500μs

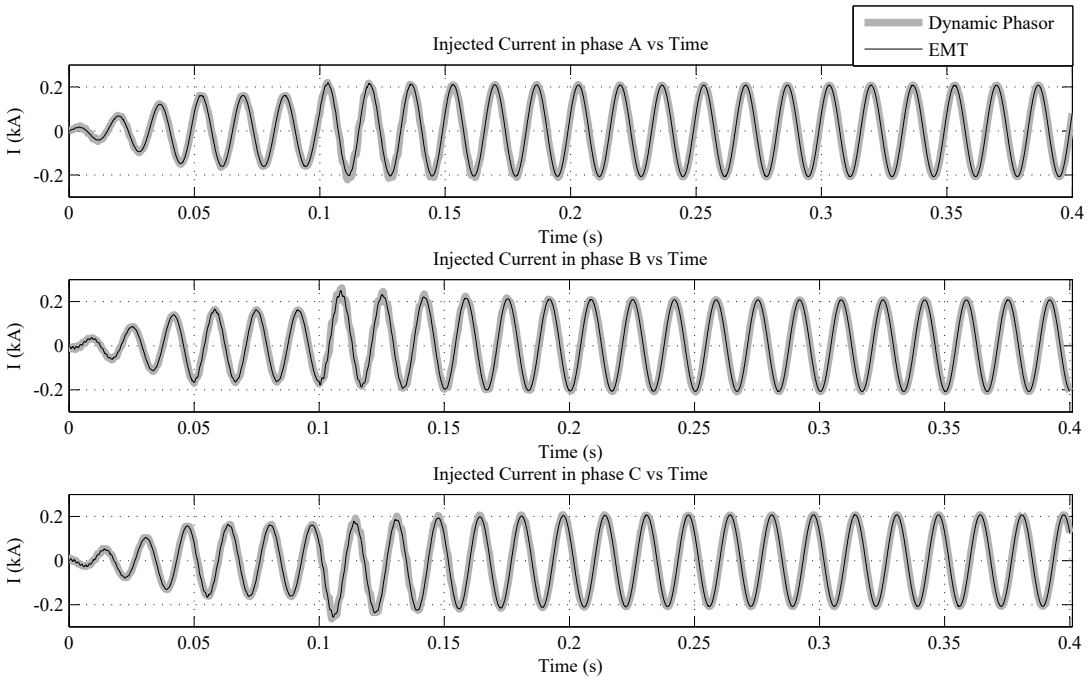

FIGURE 4.8: The injected currents to the node 3 with the time step of 500μs

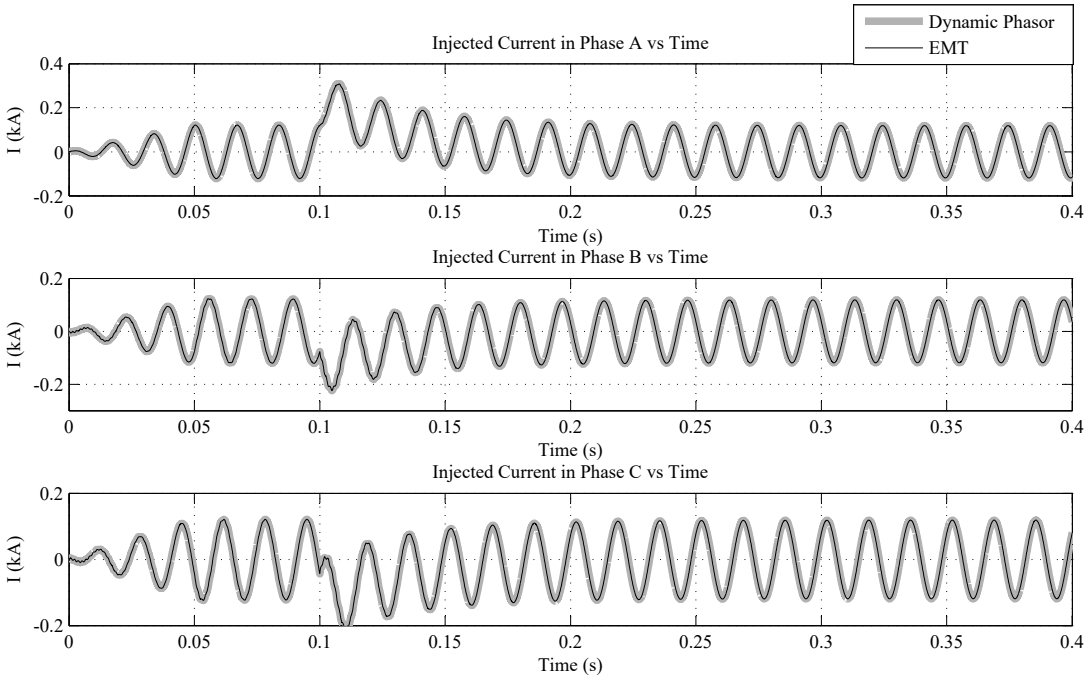

FIGURE 4.9: The injected currents to the node 1 with the time step of 50μs

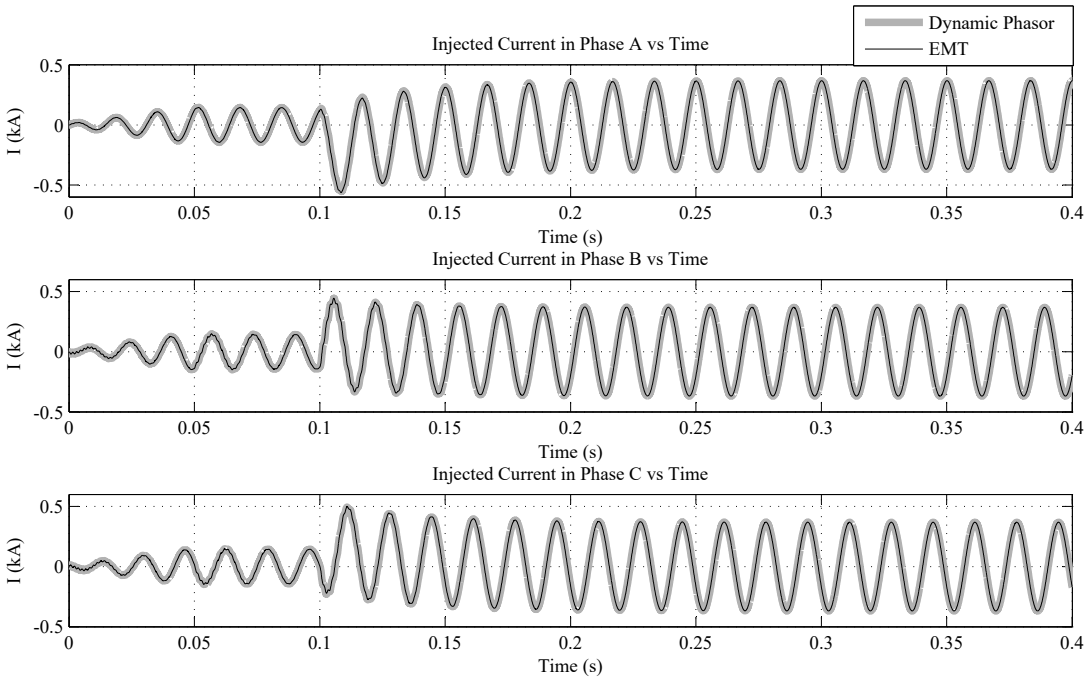

FIGURE 4.10: The injected currents to the node 2 with the time step of 50μs

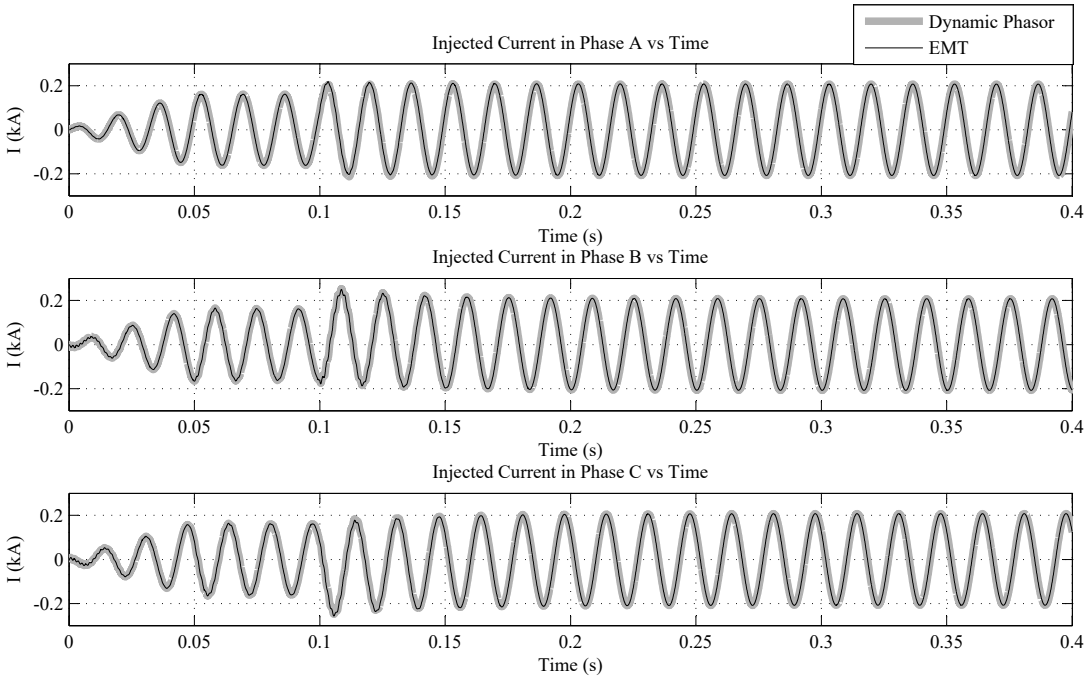

FIGURE 4.11: The injected currents to the node 3 with the time step of 50μs

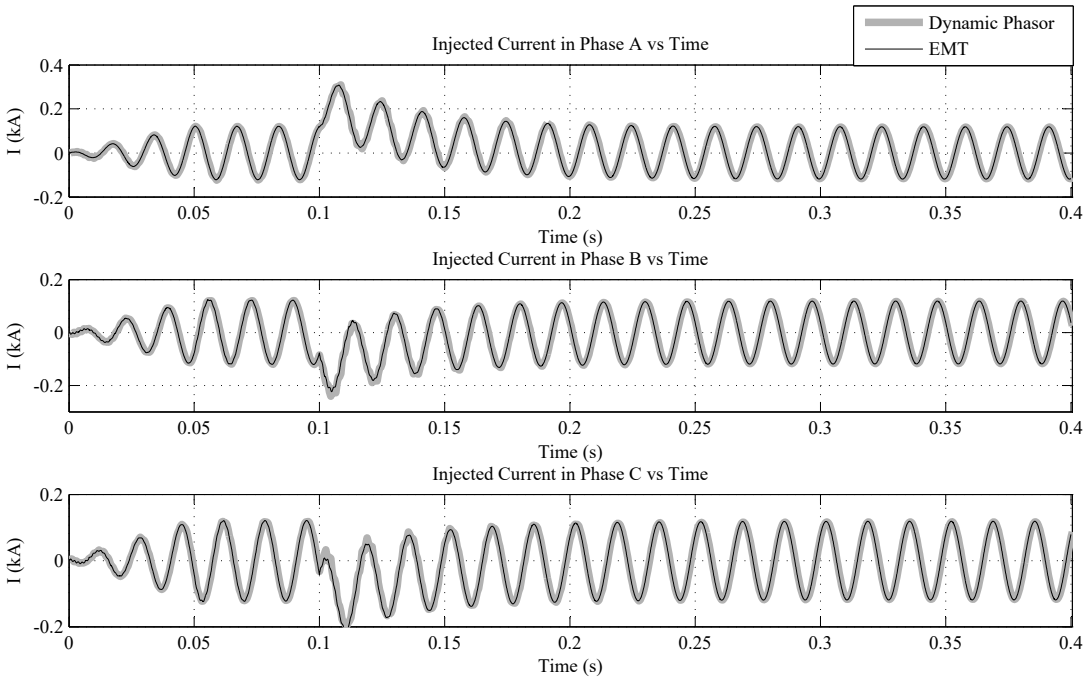

FIGURE 4.12: The injected currents to the node 1 with the time step of 500μs

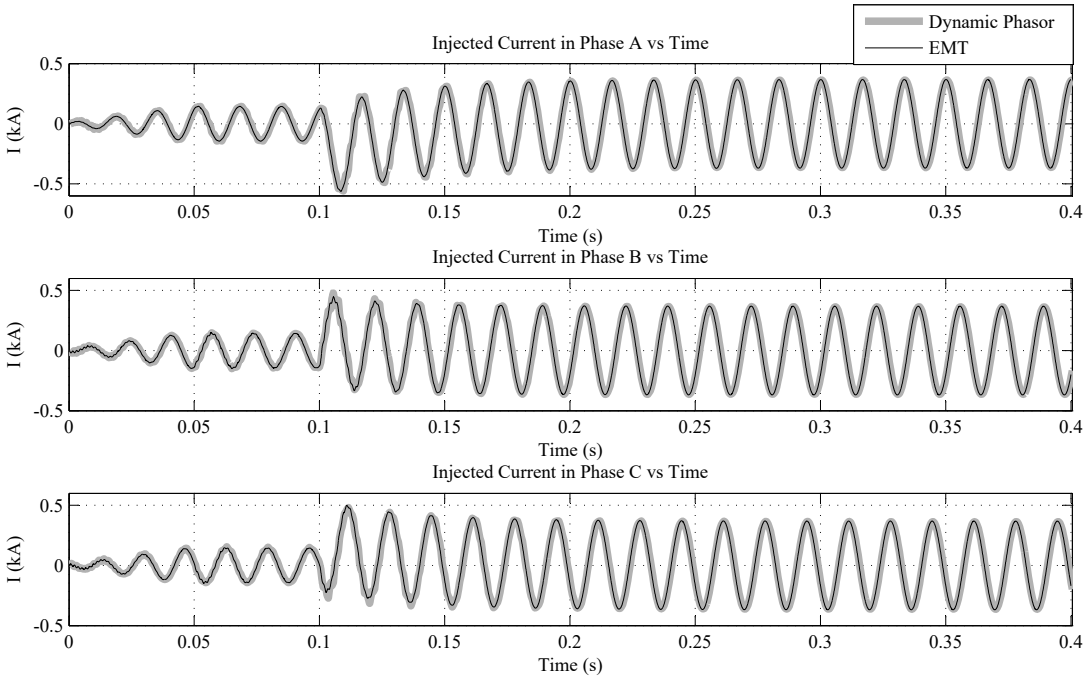

FIGURE 4.13: The injected currents to the node 2 with the time step of 500μs

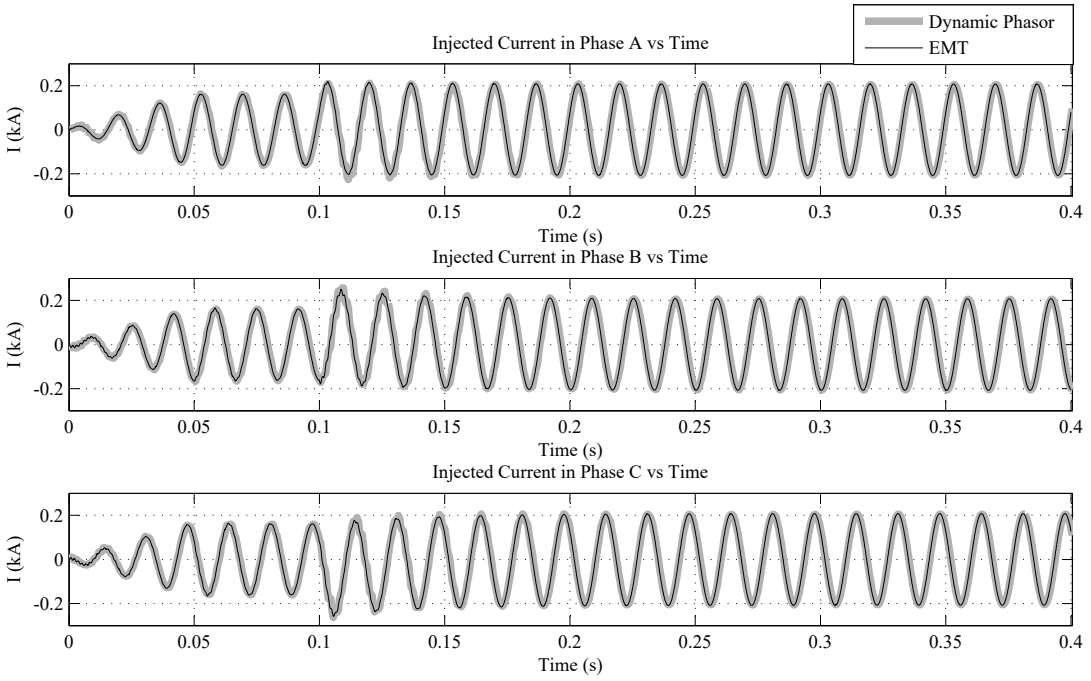

FIGURE 4.14: The injected currents to the node 3 with the time step of 500μs

4.2.3 Summary of Findings

Considering the results observed so far, it can be concluded that the dynamic phasor equivalent can adequately model the given power system. This proposed method has been tested for a five bus system but it can be easily expanded into a system containing more buses and RL/RC branches as the methodologies presented in Section 3.2 and Section 3.3 are general approaches independent of number of nodes. The simulation can also been carried out using a higher time step ($0.5ms$) for this particular system (Figure 3.1).

The two methods, state space model and the nodal analysis give similar results. Therefore, it can be established that the both methods are equally accurate. But considering the algorithm for these two models the nodal analysis is easier to generalize for a large power system.

So far balanced harmonics free voltages were considered as the input to the dynamic phasor program. In a simulation study, sometimes it is needed to apply unbalanced faults in the EMT side of the model. However, the PLL angle information can be easily corrupted by distorted voltage inputs. A positive sequence filter is proposed to eliminate the effect of the voltage unbalance. This topic will be further discussed in the next chapter.

Chapter 5

Implementation of Positive Sequence Filters to Improve the Performances of SRF-PLL in an Unbalanced Power System

For simulation studies it is necessary to analyse the system behaviour under distorted voltage conditions. The voltage and current harmonic distortions and voltage unbalanced conditions must be simulated in order to identify their effect on power system components. Therefore, the developed hybrid model should be able to model these distortions to accurately model the system behaviour. In this study the distortions in the EMT side of the model is considered since that part of the network is modelled in detailed. This will results the inputs of the dynamic phasor model to become unbalanced. In this section the voltage unbalance condition is explained, effect of this in the SRF-PLL is analysed and the solutions to mitigate the problem is discussed.

A three phase power system is called balanced or symmetrical system if the voltage magnitudes of the three phases are equal and their phases are 120^0 apart from one other. If the above conditions are not met, that power system is an unbalanced or an asymmetrical system. Unbalanced system can be a result of an unbalanced load, single phase loads or an asymmetrical fault. According to the Fortescue's theorem an unbalanced system can be resolved to three balanced systems using symmetrical components. This allows the user to analyse an unbalanced three phase power system using three balanced systems. According to this theorem a three phase voltage can be expressed as a summation of three balanced voltages.

$$V_a = V_{a0} + V_{a1} + V_{a2} \tag{5.1}$$

$$V_b = V_{b0} + V_{b1} + V_{b2} \tag{5.2}$$

$$V_c = V_{c0} + V_{c1} + V_{c2} \tag{5.3}$$

Here V_{a0} is the zero sequence component, V_{a1} is the positive sequence component and V_{a2} is the negative sequence component of the voltage V_a. In a positive sequence system, phase rotates in counter clock wise in phase sequence $a \rightarrow b \rightarrow c$. The negative sequence components are rotates in clock wise in phase sequence $a \rightarrow c \rightarrow b$. The zero sequence system is a stationary system where the angles between the three phases are zero. V_a, V_b and V_c can be written using sequence components as in (5.4), where $a = e^{j2\pi/3}$.

$$\begin{pmatrix} V_a \\ V_b \\ V_c \end{pmatrix} = \frac{1}{3} \begin{pmatrix} 1 & 1 & 1 \\ 1 & a^2 & a \\ 1 & a & a^2 \end{pmatrix} \begin{pmatrix} V_{a0} \\ V_{a1} \\ V_{a2} \end{pmatrix} \tag{5.4}$$

5.1 Performance of the PLL in an Unbalanced Power System

The SRF-PLL discussed in Chapter 5 is fast and accurate and has a simple structure. In the SRF-PLL the feedback loop of the controller is closed through a rotating reference frame (dq frame). The position of this reference frame is derived by regulating the d component into zero. For an unbalanced system, a second reference frame rotating in the opposite direction will be needed to track the negative sequence component [22]. Therefore, the SRF-PLL gives inaccurate results during a voltage unbalance. In this research a positive sequence filter is suggested to filter the positive sequence component of an unbalanced signal before feeding it into the SRF-PLL.

A number of options were considered to filter out the positive sequence signal [23]. Two of the PLL structures with positive sequence filters (i) sinusoidal signal integrator phase locked loop (SSI-PLL) [24]; and (ii) extended phase locked loop (extended PLL) [25] were selected and implemented in this study. These two methods were selected for their simplicity and the lesser computational time. Both of these methods were implemented in MATLAB and results were compared with each other.

5.2 Sinusoidal Signal Integrator Phase Locked Loop

Sinusoidal signal integrator tracks the positive sequence component of an unbalanced signal and feeds it to the SRF-PLL. Consider a positive sequence signal

where alpha component leads beta component by 90 degrees.

$$e_\alpha(t) = A\cos(\omega t + \phi) \tag{5.5}$$

$$e_\beta(t) = A\sin(\omega t + \phi) \tag{5.6}$$

The amplitude integration of $e_\beta(t)$ can be written as,

$$y_\beta(t) = A\big[\sin(\omega t + \phi)\big]t \tag{5.7}$$

Taking the Laplace transformation of the signal $y_\beta(t)$,

$$Y_\beta(s) = \frac{s}{s^2+\omega^2}\left(\frac{A\omega\cos\phi}{s^2+\omega^2} + \frac{As\sin\phi}{s^2+\omega^2}\right) + \frac{\omega}{s^2+\omega^2}\left(\frac{As\cos\phi}{s^2+\omega^2} + \frac{A\omega\sin\phi}{s^2+\omega^2}\right) \tag{5.8}$$

Similarly the Laplace transformation of the signals $e_\alpha(t)$ and $e_\beta(t)$ can be written as,

$$E_\alpha(s) = \frac{As\cos\phi}{s^2+\omega^2} - \frac{A\omega\sin\phi}{s^2+\omega^2} \qquad E_\beta(s) = \frac{A\omega\cos\phi}{s^2+\omega^2} + \frac{As\sin\phi}{s^2+\omega^2} \tag{5.9}$$

Considering these three equations it can be seen that the signal $Y_\beta(s)$ can be constructed using $E_\alpha(s)$ and $E_\beta(s)$.

Now consider the alpha component of the positive sequence signal. The amplitude integration of $e_\alpha(t)$ can be written as,

$$y_\alpha(t) = A\big[\cos(\omega t + \phi)\big]t \tag{5.10}$$

Taking the Laplace transformation of the signal $y_\alpha(t)$,

$$Y_\alpha(s) = \frac{-\omega}{s^2+\omega^2}\left(\frac{A\omega\cos\phi}{s^2+\omega^2} + \frac{As\sin\phi}{s^2+\omega^2}\right) + \frac{s}{s^2+\omega^2}\left(\frac{As\cos\phi}{s^2+\omega^2} + \frac{A\omega\sin\phi}{s^2+\omega^2}\right) \tag{5.11}$$

The signal $Y_\alpha(s)$ also can be constructed using $E_\alpha(s)$ and $E_\beta(s)$.

The same approach can be used to derive the equations for a negative sequence signal. Using these equations for a positive sequence signal the positive sequence integrator can be implemented as Figure 5.1-A and for a negative sequence signal the negative sequence integrator can be implemented as Figure 5.1-B.

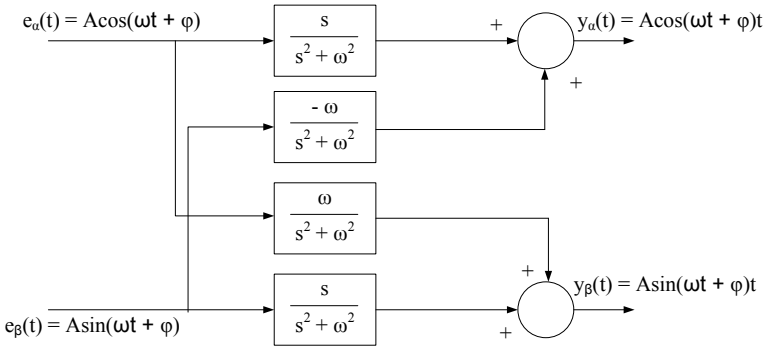

(A) Positive sequence signal passing through a positive sequence integrator

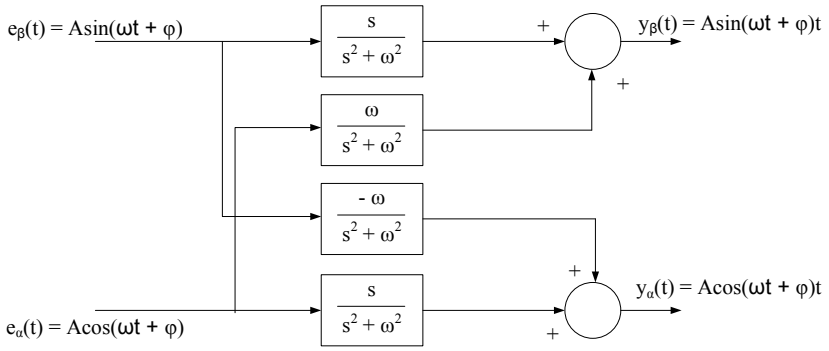

(B) Negative sequence signal passing through a negative sequence integrator

FIGURE 5.1: Positive and negative sequence integrators

Figures 5.2 A and B show a positive sequence signal passing through a negative sequence integrator and a negative sequence signal passing through a positive sequence integrator. By comparing the outputs of these set-ups and the previous set-ups (Figure 5.1-A and B), it can be seen that when a negative sequence signal going through a positive sequence integrator the output is negligible

compared to the output when a positive sequence signal going through a positive sequence integrator [24].

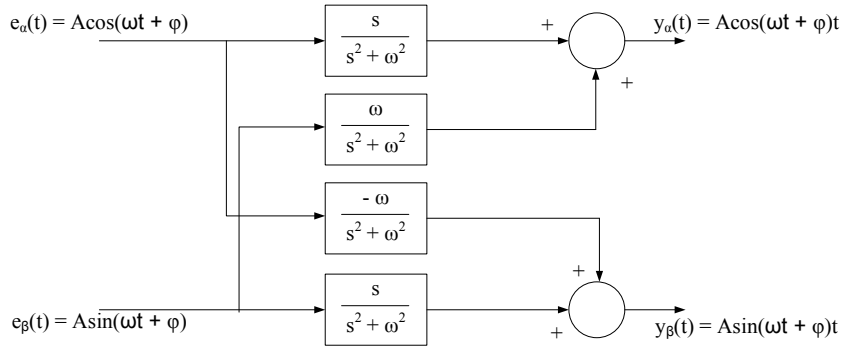

(A) Positive sequence signal passing through a negative sequence integrator

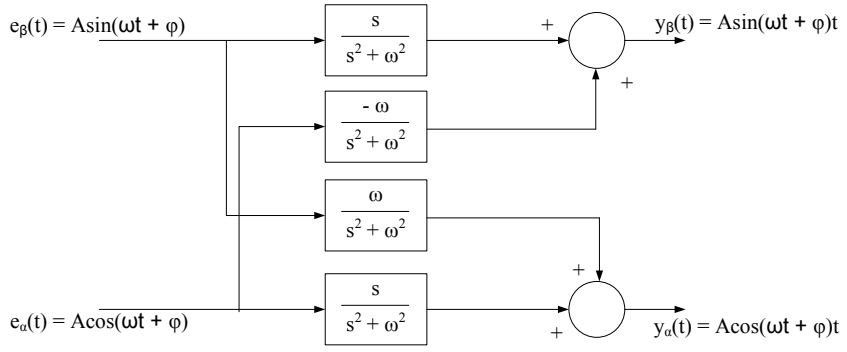

(B) Negative sequence signal passing through a positive sequence integrator

FIGURE 5.2: Positive and negative sequence integrators giving neglegible outputs

Considering this important observation, it is evident that if an unbalanced signal that has positive and negative sequence components is sent through a positive sequence integrator the output will contain only the amplitude integration of the positive sequence signal. Based on this theory a sequence filter has been implemented to extract the positive sequence signal from an unbalanced signal (Figure 5.3). The filter gain k controls the bandwidth and the response speed of the filter.

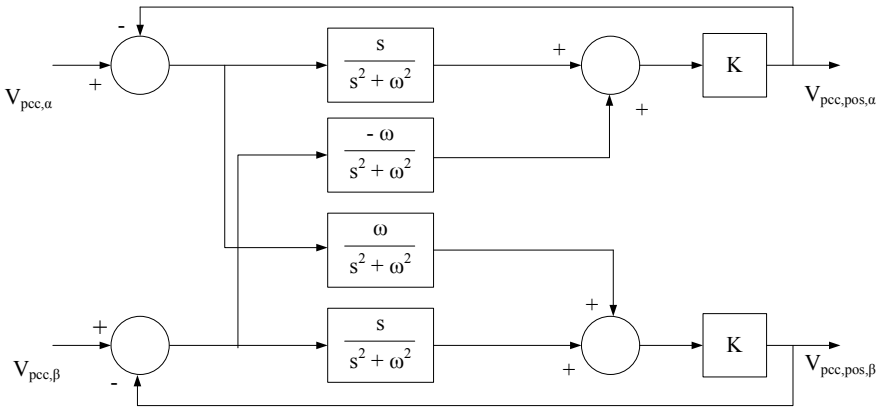

FIGURE 5.3: Sequence filter to extract the sinusoidal positive sequence signal from an unbalanced signal

Behaviour of SSI PLL in a Voltage Unbalance

The filter gain "k" has a significant impact on the filter performance. The Figure 5.4 shows the filter behaviour for different "k" values. For this, the same magnitude of positive sequence and negative sequence signals were generated and sent through the filter. Equations (5.12), (5.13) and (5.14) are the generated three phase signal inputs. These equations were converted to it's alpha-beta components and sent to the sequence filter.

$$V_a = V_m \sin(\omega_0 t) + V_m \sin(-\omega_0 t + \theta) \tag{5.12}$$

$$V_b = V_m \sin(\omega_0 t - 2\pi) + V_m \sin(-\omega_0 t - 2\pi + \theta) \tag{5.13}$$

$$V_c = V_m \sin(\omega_0 t + 2\pi) + V_m \sin(-\omega_0 t + 2\pi + \theta) \tag{5.14}$$

After analysing the output waveforms it was clear that when the value of "k" increases the speed of the filter increases. On the other hand higher "k" values lead to a steady state error in the output. It was understood that when "k" has a high value, the filter cannot completely suppress the negative sequence

component at the output.

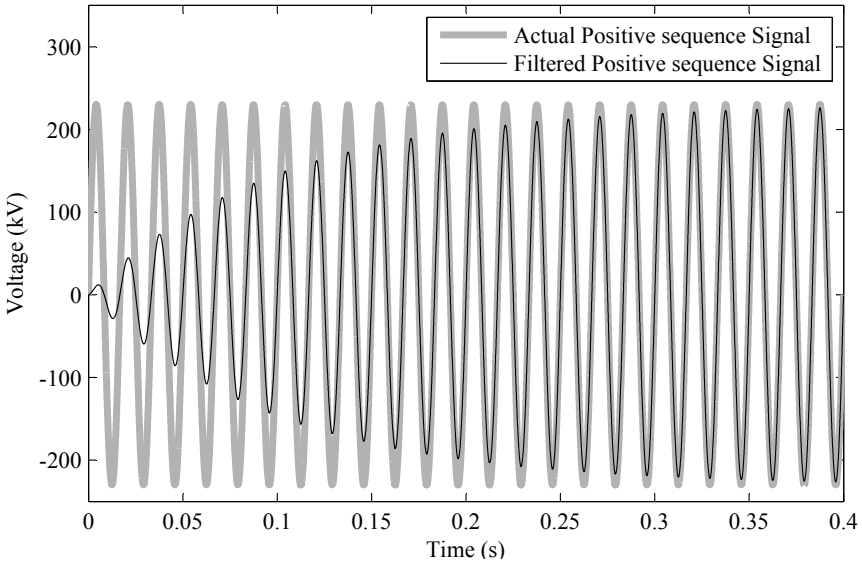

(A) Positive sequence of the alpha component of the three phase voltage for k=10

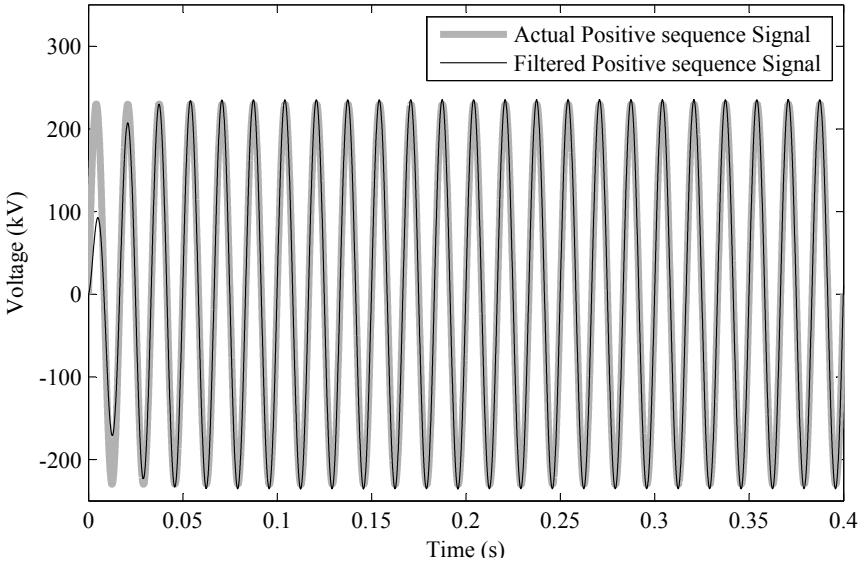

(B) Positive sequence of the alpha component of the three phase voltage for k=100

FIGURE 5.4: Sequence filter behaviour for different values of filter gain

5.3 Extended Phase Locked Loop

Extended PLL uses the concept of symmetrical components to resolve an unbalanced system to its positive sequence [26]. The symmetrical components are defined in phasors and they can be converted to time domain signals by replacing the phase shift operator "a" by 120^0 phase shift in time domain [27]. For the ease of implementation 120^0 phase shift is expressed using the 90^0 phase shift as in (5.16) [25].

$$\begin{pmatrix} v_{a1}(t) \\ v_{b1}(t) \\ v_{c1}(t) \end{pmatrix} = \frac{1}{3} \begin{pmatrix} 1 & a & a^2 \\ a^2 & 1 & a \\ a & a^2 & 1 \end{pmatrix} \begin{pmatrix} v_a(t) \\ v_b(t) \\ v_c(t) \end{pmatrix} \tag{5.15}$$

$$a = e^{j120} = -\frac{1}{2} + \frac{\sqrt{3}}{2} e^{j90} \tag{5.16}$$

$$v_{a1}(t) = \frac{1}{3} * v_a(t) - \frac{1}{6}\big(v_b(t) + v_c(t)\big) - \frac{1}{2\sqrt{3}} e^{j90}\big(v_b(t) - v_c(t)\big) \tag{5.17}$$

$$v_{b1}(t) = -v_{a1}(t) - v_{c1}(t)) \tag{5.18}$$

$$v_{c1}(t) = \frac{1}{3} * v_c(t) - \frac{1}{6}\big(v_a(t) + v_b(t)\big) - \frac{1}{2\sqrt{3}} e^{j90}\big(v_a(t) - v_b(t)\big) \tag{5.19}$$

The 90^0 phase shift operator can be represented by an all pass filter which generates a 90^0 phase shift at the center frequency [26]. A simple first order filter was used for this purpose. The transfer function of the filter H(ω) is,

$$H(\omega) = \frac{1 - s/\omega_0}{1 + s/\omega_0} \tag{5.20}$$

The block diagram of the extended PLL is shown in the Figure 5.5 [26].

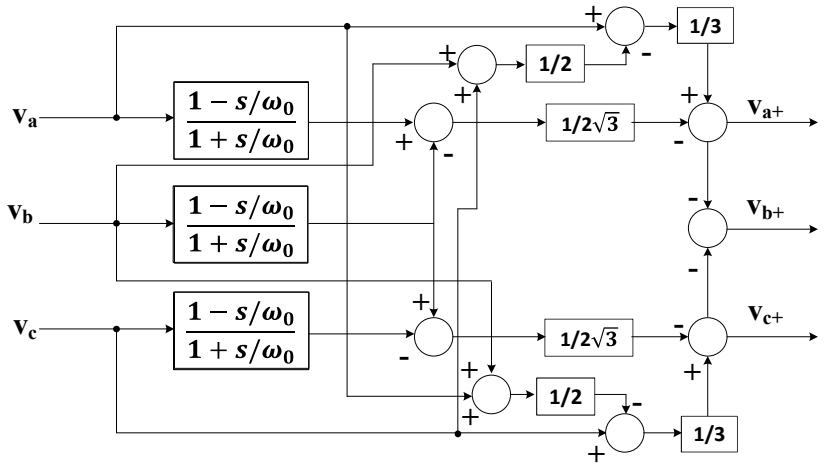

FIGURE 5.5: The structure of the extended PLL

Behaviour of Extended PLL in a Voltage Imbalance

The Figure 5.6 shows the performances of the extended PLL when extracting the positive sequence signal from the same unbalanced signal used for the SSI-PLL in the Section 5.2. It can be seen from the figure that there is zero steady state error involved in an extended PLL. Also, the filter speed is relatively high.

5.4 Comparison of Results of the Phase Locked Loop Structures

In this section, a comparison between the performance of SRF-PLL, SSI-PLL and extended PLL is presented. The evaluation is done by considering the PLL error, estimated phase angle and the estimated phasor voltages. To evaluate the performances of the three PLL structures, three phase balanced voltages were created as the input and from $t = 0.2s$ to $0.3s$, a negative sequence voltages were

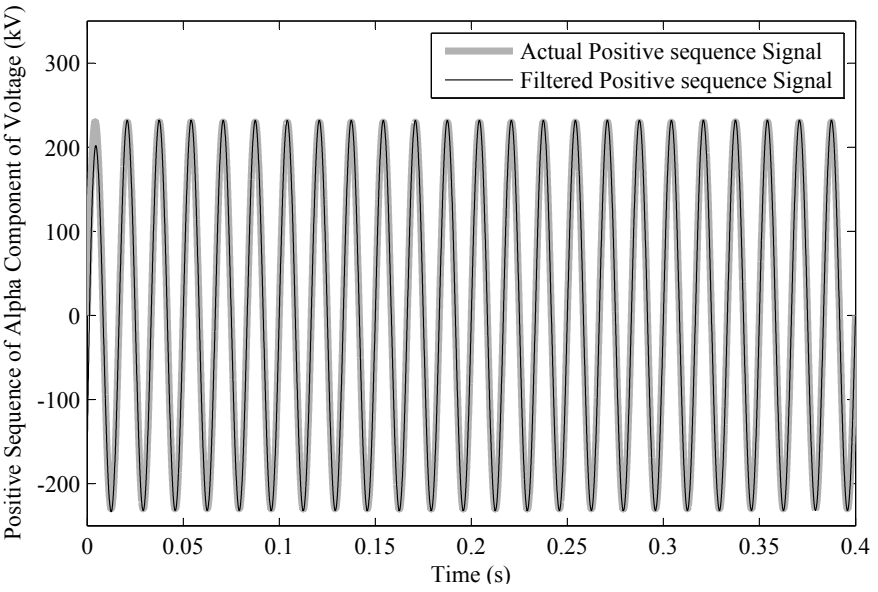

FIGURE 5.6: Performances of the extended PLL

added to make the system unbalanced. The same magnitude of negative sequence component was added to the three phase signal at $0.2s$.

First, the conventional PLL was evaluated against the voltage unbalance and the PLL error is plotted in Figure 5.7. It can be seen that when a voltage unbalance happens the PLL error tends to go towards a large value which will lead to erroneous results in a simulation. Next, the PLL error of the extended PLL and the SRF-PLL are plotted in Figure 5.8. Both the SRF-PLL and extended PLL has better performance compared to the conventional PLL. Extended PLL has less oscillations in a voltage unbalance compared to SSI-PLL. However there is a high transient error in extended PLL at the point where the voltage became unbalanced. Figure 5.9 shows the angle estimation of the three PLL systems. Figure 5.10 and Figure 5.11 show the estimated phasor values of the voltages. Initially SSI-PLL has taken a long time to achieve the steady state. Therefore, it can be said that the SSI-PLL is relatively slow compared to the extended PLL. Also the extended PLL response is better damped. The performances of the three

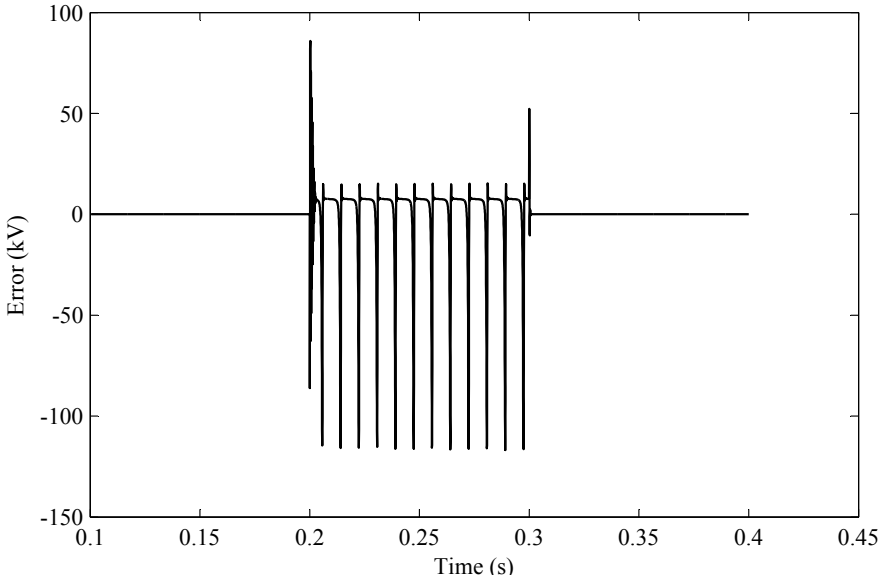

FIGURE 5.7: Error Signal of the SRF-PLL in a voltage unbalance

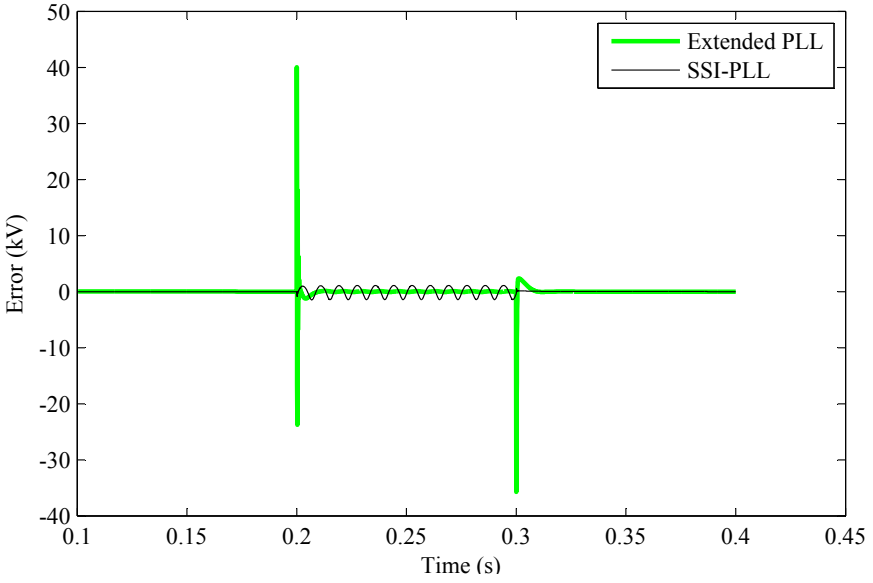

FIGURE 5.8: Comparison of the PLL error of SSI-PLL and extended PLL

PLL structures are compared in the Table 5.1 [10].

TABLE 5.1: Comparison of the PLL Structures

Method	**Speed**	**Unbalance**	**Complexity**	**Tuning**
PLL	Very Fast	Poor	Simple	Easy
SSI-PLL	Moderate-Slow	Moderate	Moderate	Moderate
Extended PLL	Fast	Good	Simple	Easy

Considering the results it can be concluded that the extended PLL has better performance compared to the SSI-PLL. Extended PLL involves zero steady state error and the filter speed is acceptable. It is hard to tune the filter gain "k" of the SSI-PLL to get the same performance as extended PLL. However, the extended PLL has following limitations [26].

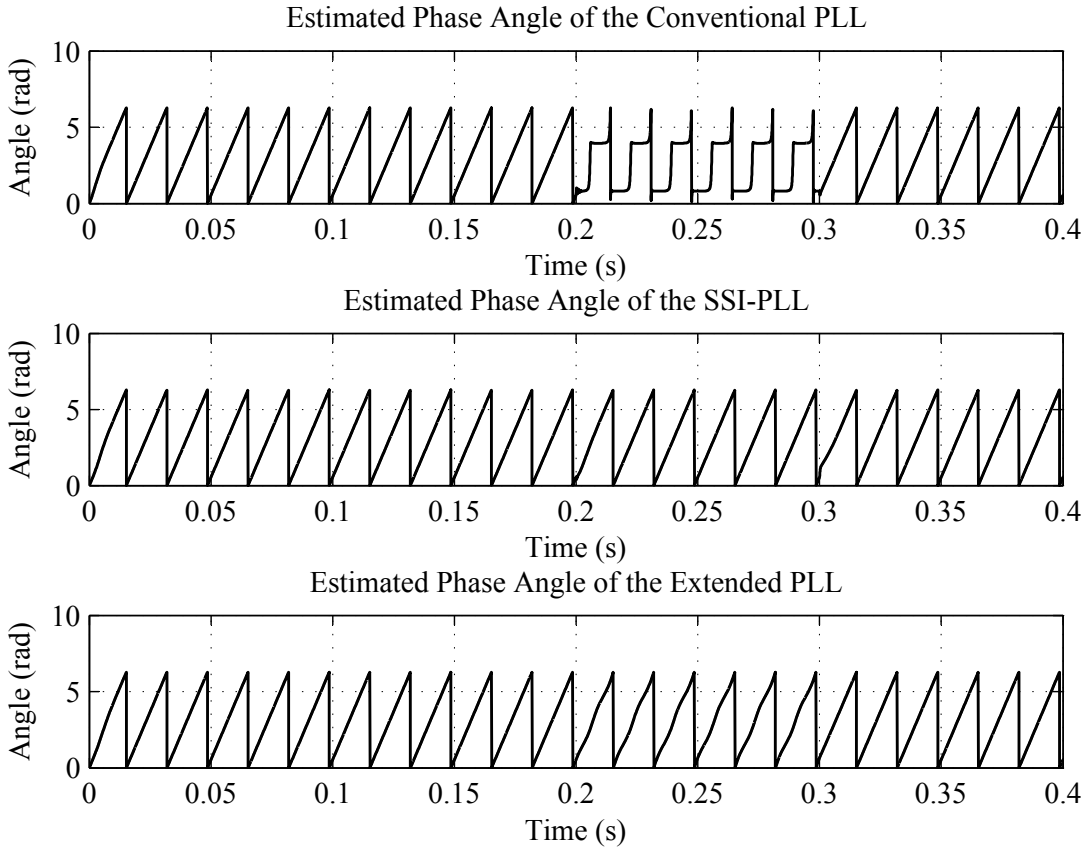

FIGURE 5.9: Comparison of the PLL angle of SRF-PLL, SSI-PLL and extended PLL

- All pass filters are not frequency adaptive. Therefore, they do not work properly when the center frequency of the simulation changes. The enhanced PLL [26] and three-phase magnitude phase locked loop [28] are some of the methods suggested to improve this problem. These are frequency adaptive PLL structures that can track the magnitude, phase angle, and frequency of the utility voltage.

- Extended PLL does not block harmonics and distortions.

The harmonics and other distortions can be removed by reducing the bandwidth of the PLL. But this will reduce the speed of the loop filter in the PLL [29]. Therefore, a low pass filter is recommended for better performances under distorted EMT side network conditions.

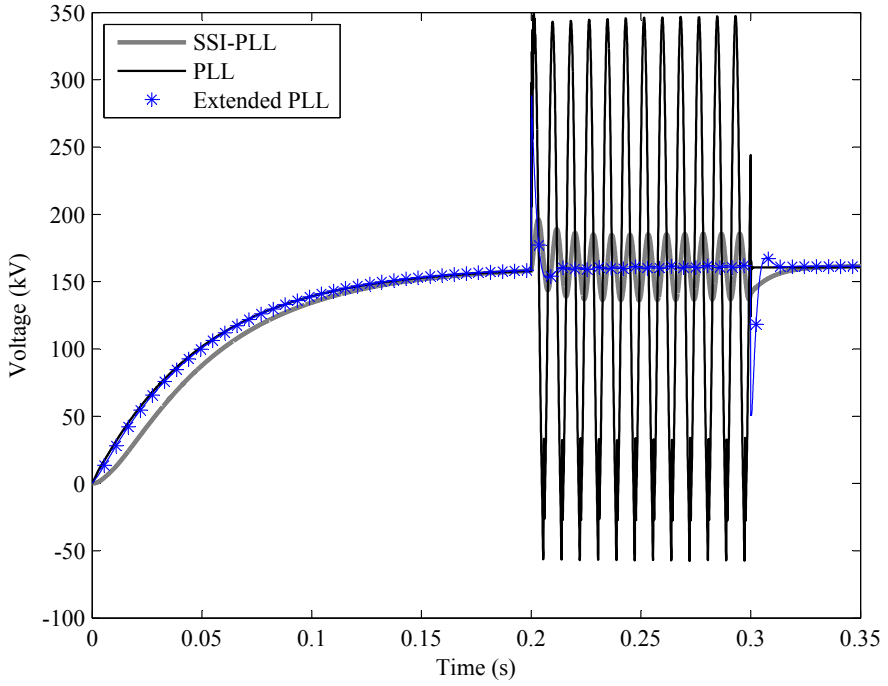

FIGURE 5.10: Comparison of the real part of the voltage output of conventional SRF PLL, SSI-PLL and extended PLL

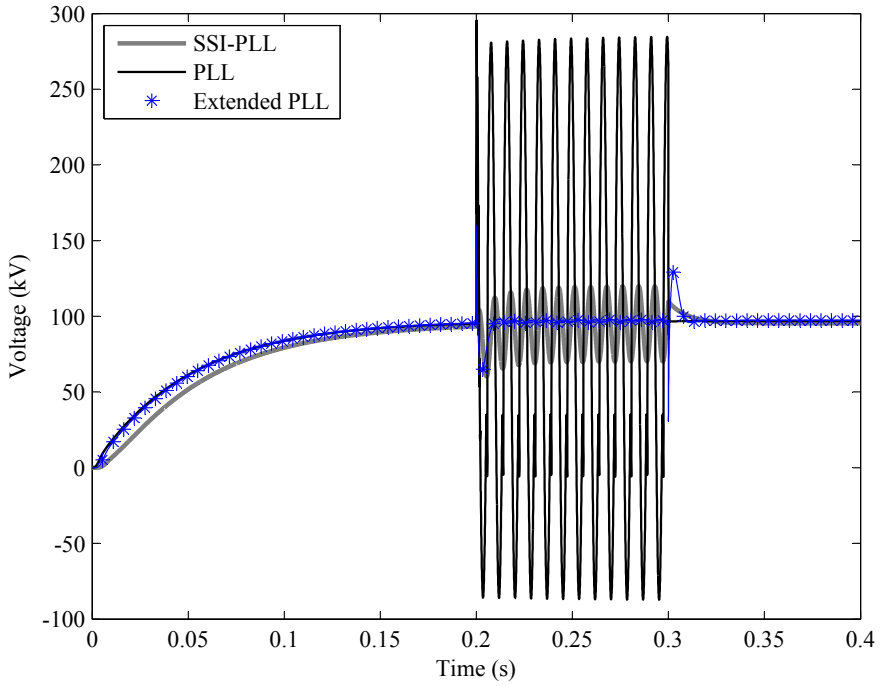

FIGURE 5.11: Comparison of the imaginary part of the voltage output of conventional SRF PLL, SSI-PLL and extended PLL

The effect on the PLL from the zero sequence of an unbalanced system is eliminated by adding a pre-filter which is designed to remove the zero sequence component. Zero sequence component of an unbalanced system can be obtained by the following equation.

$$V_{a0} = V_{b0} = V_{c0} = \frac{1}{3}\big(V_a + V_b + V_c\big) \tag{5.21}$$

By removing the resultant of (5.21) from the input signal, PLL can track the positive sequence component of the fundamental wave under distorted utility conditions.

5.5 Summary

The performance of two positive sequence filters were evaluated in this chapter. It was concluded that the extended PLL has better performance compared to SSI-PLL in a voltage unbalance. Taking this into the account, the extended PLL was selected as the interface between the dynamic phasor equivalent and the EMT model. A pre-filter was added before the extended PLL to remove the zero sequence of the input signal. The complete block diagram of the proposed system for converting three phase instantaneous values to its phasor domain is shown in the Figure 5.12.

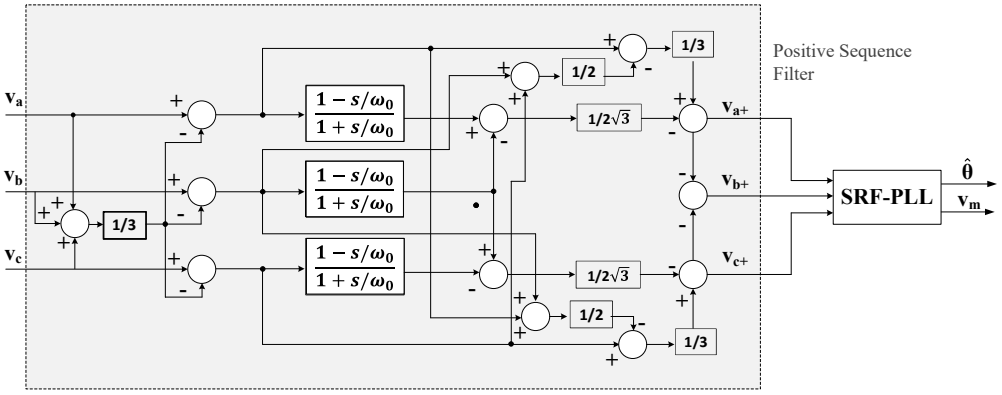

FIGURE 5.12: Complete block diagram for detecting the phasor quantities from a three phase signal

Chapter 6

Implementing Dynamic Phasor Type Solution in Real Time Digital Simulator

This chapter presents a real-time implementation of the dynamic phasor model described in Chapters 3, 4 and 5. An user defined power system component was developed to represent the dynamic phasor equivalent in RTDS.

6.1 Structure of the Proposed System

For the implementation of the dynamic phasor model, the network has to be partitioned into two parts where the smaller system containing power electronic devices, which needs detailed simulation, is simulated using EMT type simulation. The larger sub network is simulated using the dynamic phasor model. The block diagram of the proposed scheme is in Figure 6.1.

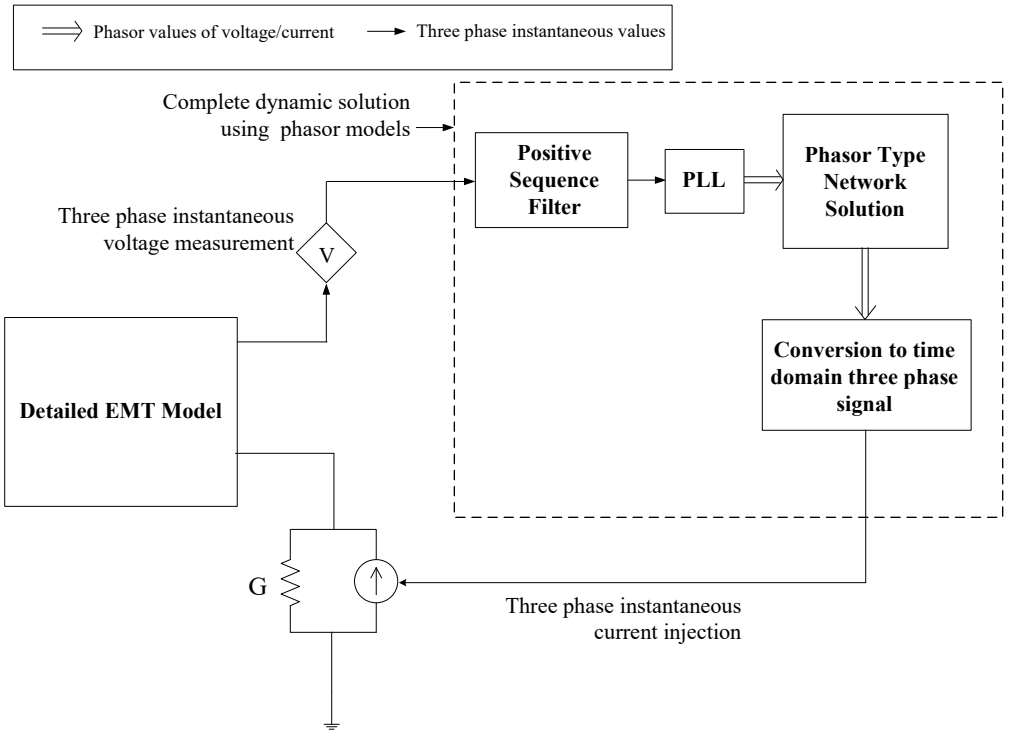

FIGURE 6.1: Structure of the proposed system

In this study, the time step of the dynamic phasor simulation is reduced to 50μs to ensure to give a solution per time step in real time simulation. The dynamic phasor type simulation is implemented in RTDS as a power system component. In RTDS power system components are modelled as a current source in parallel with a resistor. Therefore, in the dynamic phasor equivalent the interface has to be specified as a current source behind a resistor. The voltages and currents in the RTDS is three phase instantaneous values. But the dynamic phasor simulation uses real and imaginary values of voltages and currents. The set-up with the extended PLL in Figure 5.12 was used to convert this with respect to a common reference. The simulation results are presented in the following order.

1. In the hybrid simulation the EMT network was modelled as voltage sources with resistive source impedances.

2. The dynamic phasor model was connected to an EMT model containing transmission lines, machines, loads and etc..

3. Numerical instability problems in the hybrid simulation model is analysed and presented.

4. Solutions to mitigate the problem is analysed.

6.2 Hybrid System Simulation using RTDS

In this research, for ease of implementation a small network containing only five buses (Figure 3.1) was modelled using dynamic phasors. Each RL and RC branch in the network was modelled using state equations.

Since all the nodes connected to the EMT model has to be specified by a current source and a certain impedance, only the selected (coloured) part of Figure 3.1 was modelled in dynamic phasors. And the three capacitors connected to the three ends were modelled as EMT type components using the Dommel's algorithm. Dynamic phasor block contains the capacitors in the interface along with the dynamic phasor model of the rest of the external system. Then the total current to an interface node would be the addition of the current injection from the capacitor and the dynamic phasor model. The impedance parallel to the total current will be equal to "$\frac{\Delta t}{2C}$". This concept is illustrated in Figure 6.2-A. The interface to the EMT program can also done by connecting a large resistance in parallel with the current source (Figure 6.2-B), which is derived from the dynamic phasor model.

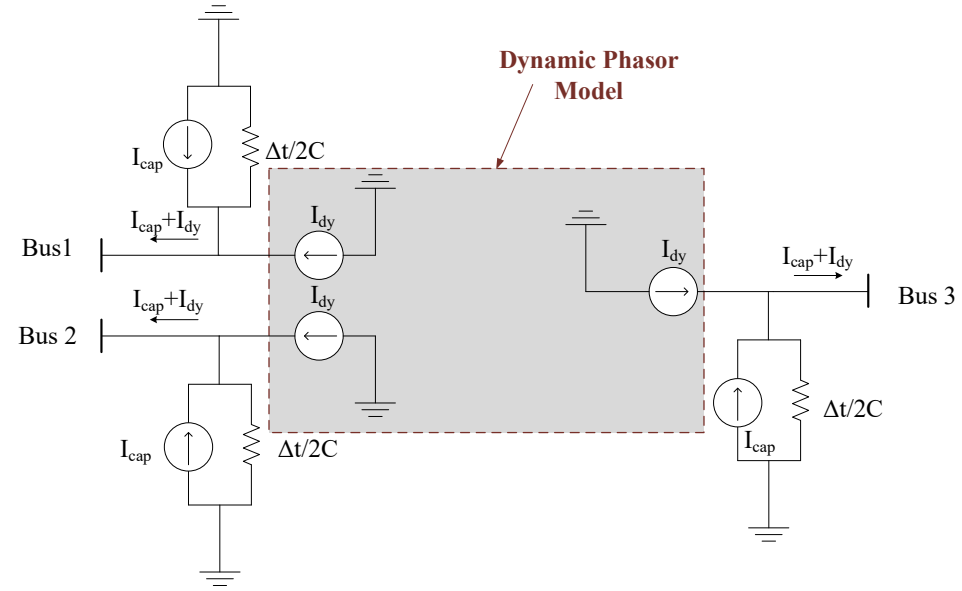

(A) Method 1

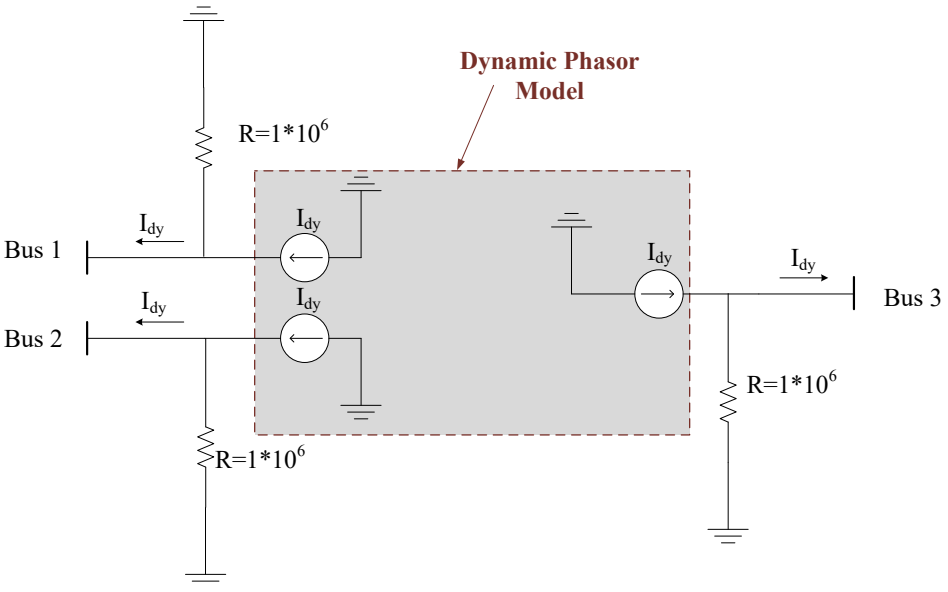

(B) Method 2

FIGURE 6.2: Interfacing the dynamic phasor model to RTDS

6.3 Simulation Results

6.3.1 Evaluation of the interface

The interface between the EMT model and the dynamic phasor equivalent is evaluated by connecting three EMT modelled voltage sources with purely resistive impedance to the interface nodes. This is illustrated in Figure 6.3. Figure 6.4

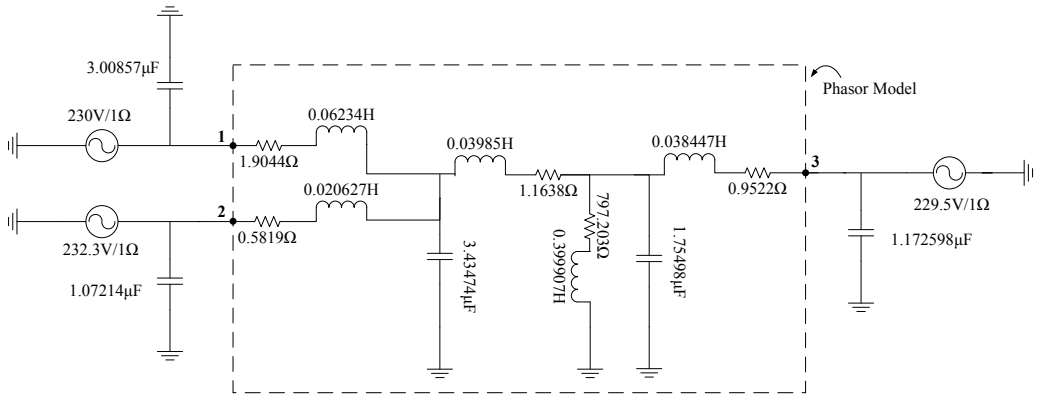

FIGURE 6.3: RTDS simulation case with three voltage sources

shows the phase "a" injected currents from dynamic phasor simulation to the EMT simulation when a phase "a" line to ground fault happen at 0.2s for a period of two cycles at one of the interface buses (node 2 of Figure 6.3). The simulation was carried out in RTDS and the results were compared against a fully EMT simulated system. Considering the Figure 6.4 it is evident that the hybrid model adequately represents the given network.

6.4 Limitations of the Proposed System

In this section the numerical issues faced when the dynamic phasor equivalent is connected to a large EMT network containing generators, transmission lines and

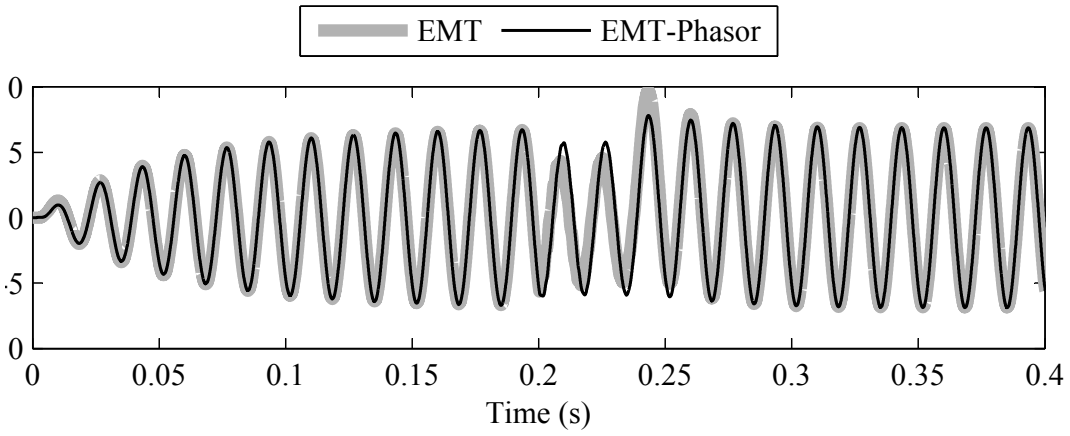

(A) Injected current into phase A of node 1

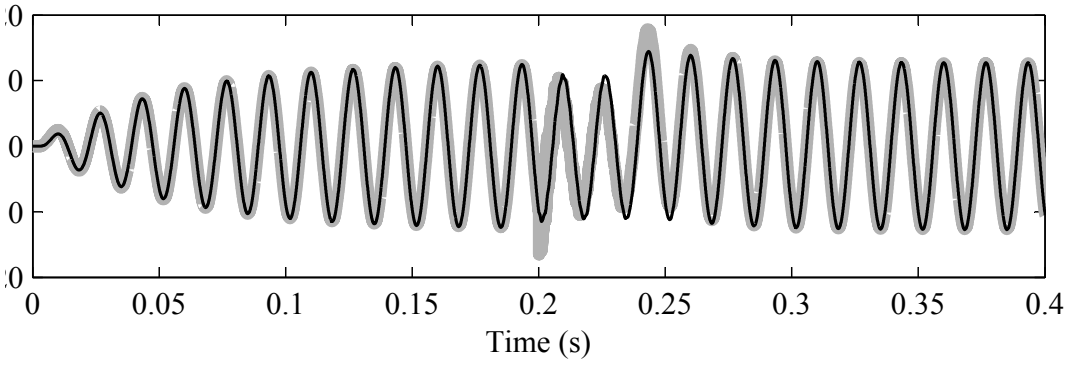

(B) Injected current into phase A of node 2

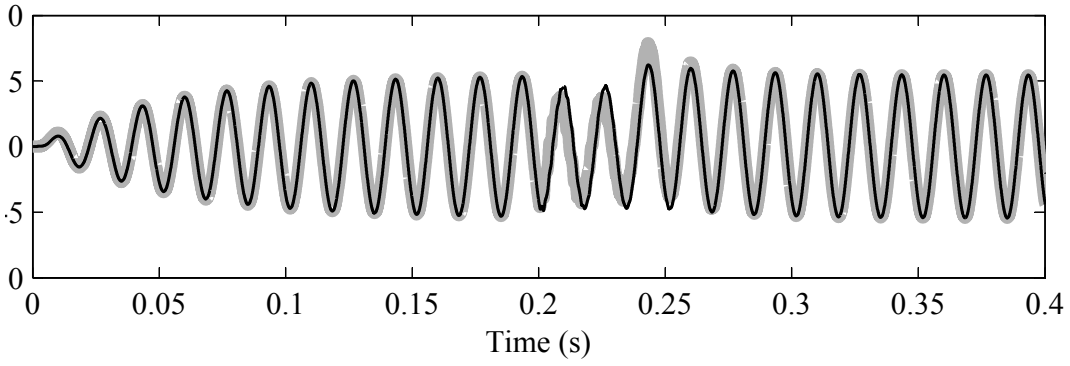

(C) Injected current into phase A of node 3

FIGURE 6.4: Comparison of results of the EMT-dynamic phasor hybrid simulated system and the fully EMT simulated system

etc. are discussed. The subsystem modelled in dynamic phasors in Figure 3.1 is connected to a large network (IEEE 68 bus system [30]) modelled in EMT model. The simulation collapsed as a result of numerical problems involved in the interface between the two models.

Networks with different types of components (inductors, capacitors etc.) were simulated using the hybrid simulator to investigate the numerical issue. After analysing the results of these simulated networks, it was understood that the numerical instability occurs when the EMT side branches connected to the interface bus has an inductor. In an EMT type simulation the currents through an inductor is considered as a state variable which can't undergo rapid changes. However, when injecting currents from the dynamic phasor model to the EMT model, the dynamic phasor model forced these inductor currents to change and this is considered to be one of the reasons for numerical instability.

The cause for numerical instability was confirmed by simulating Figure 6.3 with an inductive source impedance. The inductance value of one of the sources (the source connected to node 2) was increased by a small amount starting from zero until the simulation collapse. A shunt resistance of 4000Ω at each interface nodes was used as means of providing another path for the currents. The critical value of the inductance that the simulation worked was recorded as $L = 0.001H$. The simulation results for source inductance of 0.005H is shown Figure 6.5. Here the simulation worked well for couple of milliseconds giving same results as the EMT simulation. However, the resultant waveforms got distorted after this short period of time. Some methods suggested to improve this problem are stated below.

1. Adding a compensating resistance to the interface: The numerical instability can be a cause of the delay in updating the value of the current source representing the dynamic phasor model. Since the dynamic phasor model is

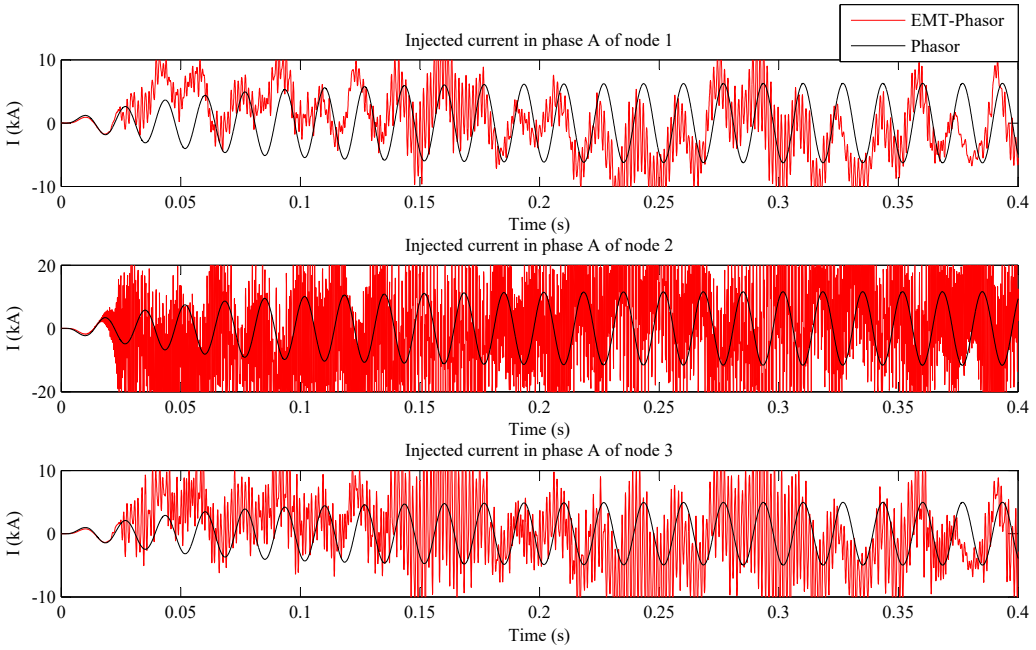

FIGURE 6.5: RTDS simulation results for source inductance of 0.0005H

not effected by the results of the EMT model until one time step later, the dynamic phasor model will work with one time step old information. The circuit in Figure 6.6 is suggested to avoid this delay [31]. This method was initially used to interface machines to the EMT program.

In this method a fictitious shunt resistance R_c is connected to the interface to avoid the open circuit condition at the interface. To compensate for the resistance, a compensation current source is added to the circuit and the value of this current source is calculated using the most recent voltage values available for the dynamic phasor model. The compensation current can be expressed as,

$$i_c = \frac{v_c(t - \Delta t)}{R_c} \tag{6.1}$$

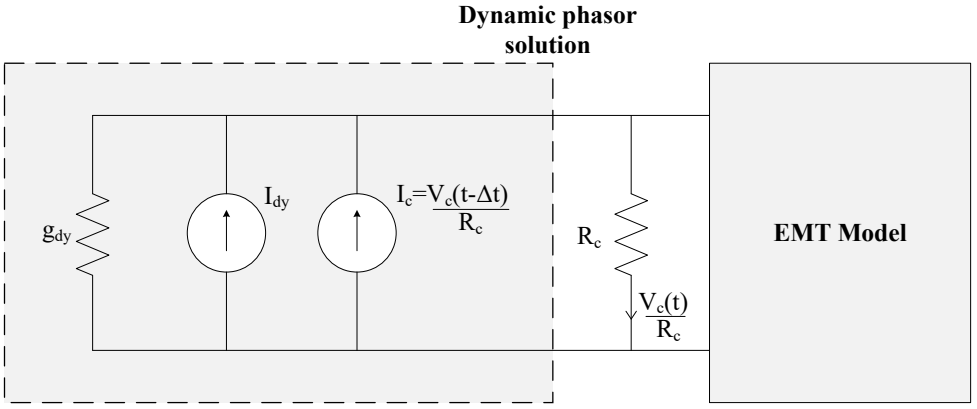

FIGURE 6.6: Interfacing the dynamic phasor solution to EMTP using a resistor with a compensation current source

Therefore, the current injection for the EMT model will be,

$$i = i_{dy} + \left(\frac{v_c(t - \Delta t)}{R_c} - \frac{v_c(t)}{R_c} \right) \tag{6.2}$$

When Δt is really small (closer to zero) the second term of (6.2) disappears so that the current to the EMT model will be equal to I_{dy} as intended. For the RTDS simulation, 50Ω shunt resistor was connected to the interface and it was compensated by adding a current source of value "$\frac{v(t)}{50}$" (where $v(t)$ is the interface point node voltage available to the dynamic phasor model). The results were improved compared to the previous time but the voltages started to distort after some milliseconds. The results of this model is shown in Figure 6.8. The hybrid model simulation results matches with the EMT model until $t = 0.15s$. At $t = 0.15s$ a numerical error started to accumulate and after some time the waveforms got distorted. Considering these observations, it can be stated that the hybrid simulation adequately model the network. However, due to numerical issues the simulation gives inaccurate results after a certain period of time.

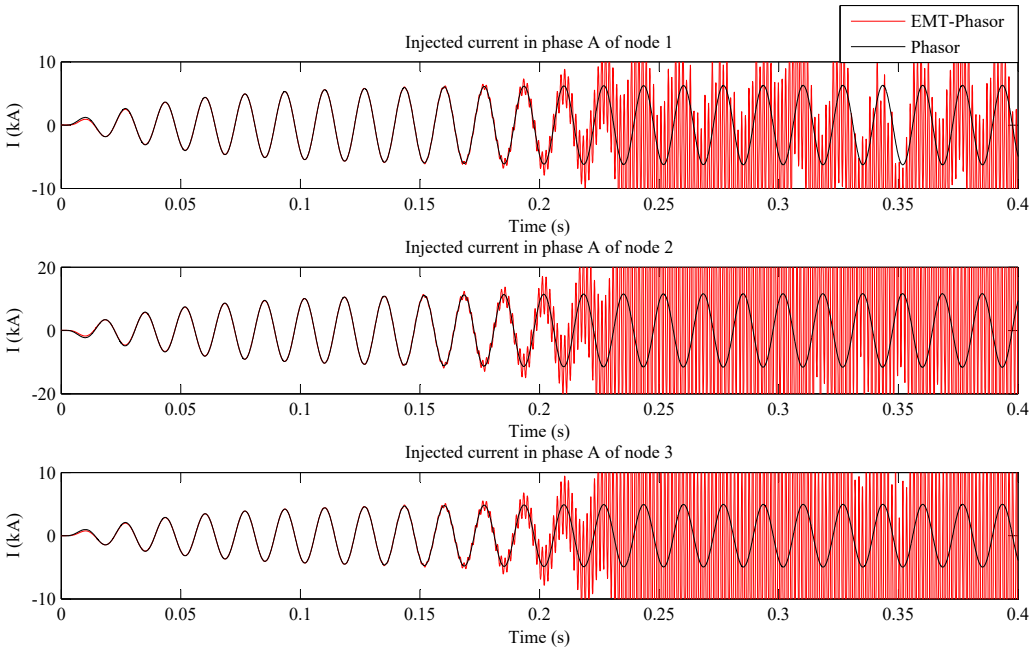

FIGURE 6.7: RTDS simulation results for source inductance of 0.0005H with a compensation current source

2. Decreasing the resistance of the shunt resistor connected to the interface assuring the network behaviour stays the same: The results for 800Ω of shunt resistance for a source inductance of $0.005H$ is shown in Figure 6.8. The same conclusion can be reached by analysing the results of this model.

3. Adding a smoothing filter to the interface so that the injection current from the dynamic phasor program will be smoothed out before it enters to the EMTP side. Injected currents to the EMT program was calculated using the previous and new values of currents as (6.3).

$$I_{dy} = (1 - k_s)I_{dy,new} + k_s I_{dy,old} \qquad 0 \leq k_s < 1 \tag{6.3}$$

A higher k_s value gives an injected current depends more on the previous

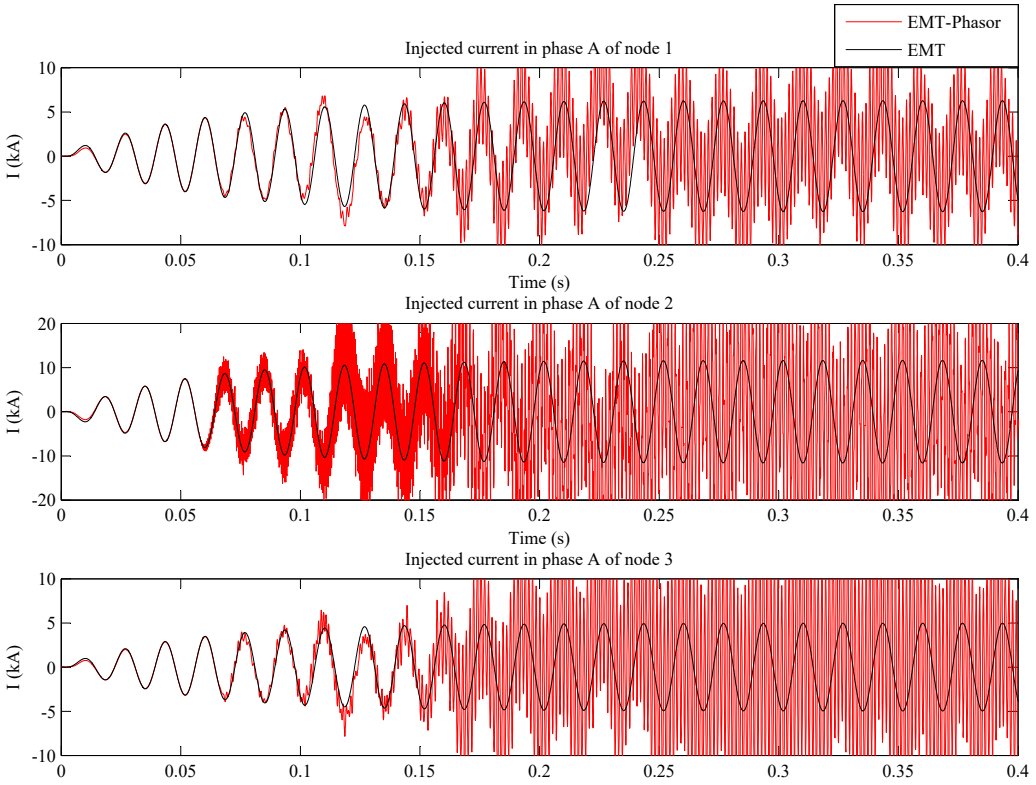

FIGURE 6.8: RTDS simulation results for source inductance of 0.0005H with a 800Ω shunt resistance at the interface

(old) value of the current. In this study, a higher k_s value has given more stable results. Figure 6.8 shows simulation results with source inductance of 0.02H with $k_s = 0.98$. Here, a shunt resistor of 1000Ω was used at the interface. The results of the hybrid simulation (Figure 6.9) can be considered accurate enough since the less important part of the network is modelled using dynamic phasors. Therefore, it can be established that the dynamic phasor model with the smoothing filter adequately represents the external system.

Although these methods mitigate numerical instability problems, more generalized solution is needed for simulating a large system. At this point, a stability analysis

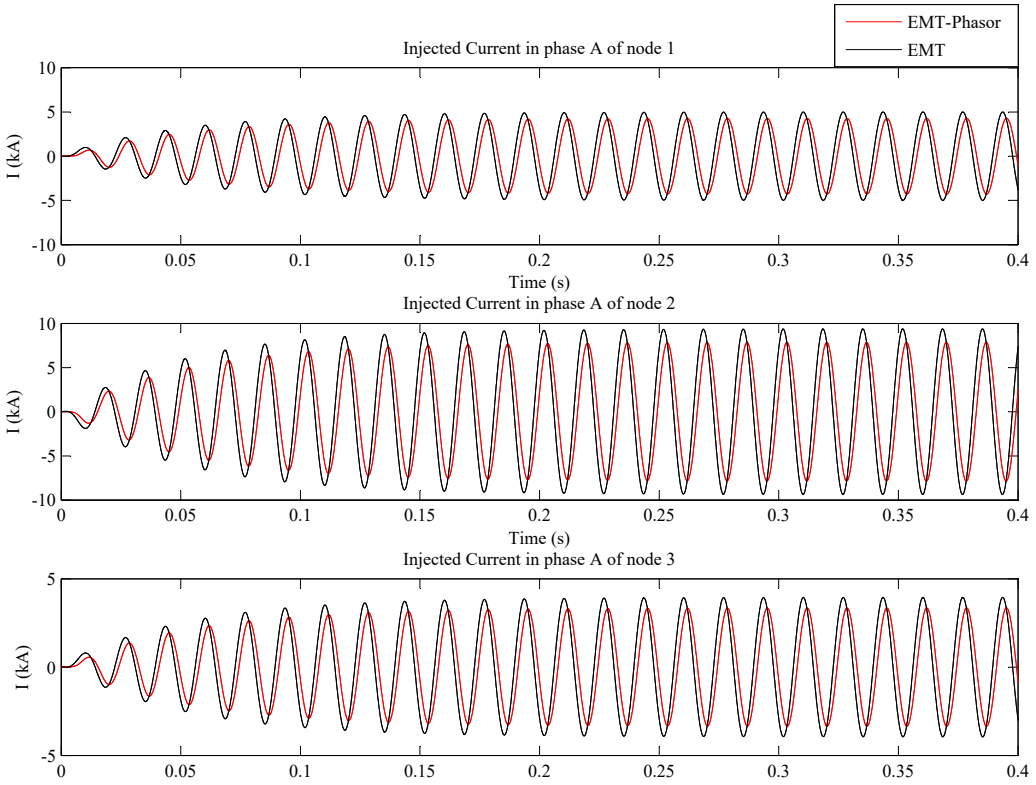

FIGURE 6.9: RTDS simulation results for source inductance of 0.02H with a smoothing filter

may needed to determine what causes the numerical instability and solutions for the problem.

Chapter 7

Conclusion and Future Work

7.1 Conclusion

A hybrid model suitable for analysing a large power system has been proposed in this thesis. The hybrid model consists of an EMT model, which was used to analyse a part of a large network in detail, and a dynamic phasor model to analyse the rest of the system. The idea of interfacing an EMT model to a dynamic phasor model is novel.

Two methods of modelling a network using dynamic phasors are presented in this thesis: state space and nodal analysis. A selected network was simulated using the two methods and the results were compared against the EMT simulation. The simulation was able to be carried out using a higher time step ($500\mu s$) compared to the electromagnetic transient simulation. Considering the results it was established that the two dynamic phasor models are equally accurate. The state space analysis is used in this study for further simulations since the simulation network considered in this study is small. However when the simulation

network expands into a large network, the nodal analysis approach is recommended since it is easy to generalize.

The SRF-PLL was suggested in this study for the interface between the EMT model and the dynamic phasor model. A dynamic phasor simulation was carried out including the SRF-PLL at the interface and the results revealed that the SRF-PLL is suitable to determine the phasors of a dynamic system. The SRF-PLL was considered robust since the PLL gains were kept constant during the simulation.

To eliminate the unbalanced effect on the SRF-PLL, a positive sequence filter was used before the SRF-PLL. Between the two positive sequence filters evaluated, the extended PLL performed better in a voltage unbalance compared to the SSI-PLL. Therefore, the extended PLL was chosen as the interface between the EMT model and the dynamic phasor model.

The hybrid model was implemented in EMT-RTDS. A small network was simulated using dynamic phasor equivalent and the system was connected to an EMT model. The hybrid model was successfully validated against a fully EMT simulated system.

One major problem of the real time EMT-dynamic phasor type simulation is the numerical instability when the EMT side simulated network expands into a large network. It was concluded that the numerical instability occurs when the EMT side branches connected to the interface bus has an inductor. In this thesis some measures were presented to mitigate the problem.

7.2 Contributions

The major contributions of this thesis are summarized below.

1. A novel hybrid simulation technique to analyse a large power system was presented. The electromagnetic transient simulation was used to simulate a part of a large network in detail and the rest of the system was modelled in dynamic phasors.

2. The synchronous reference frame phase locked loop was introduced as the interface between the EMT model and the phasor model.

3. A small network was modelled using dynamic phasors using two methods: state space analysis and nodal analysis. The results of the two models were validated against EMTP. The nodal analysis approach was recommended in this study for simulating large networks.

4. Two positive sequence filters i) sinusoidal signal integrator PLL ii) extended PLL were evaluated as the interface between the two simulation models in a voltage unbalance. A comparison of results of the two filters was carried out considering the speed, steady state error and etc.. The extended PLL was recommended to use in unbalanced conditions since it has better performance compared to the other model.

5. The hybrid system was implemented in RTDS and the performance of the hybrid model was evaluated against the EMT simulation. Based on the results of the two models, it can be concluded that the hybrid model adequately models a given network.

6. Numerical issues involved in the hybrid model was investigated when the EMT simulated network expands into a large network. Some solutions to mitigate this problem were presented.

These contributions have led to the following publication,

- H. Konara and U.D. Annakkage, "Evaluation of Two Positive Sequence Filters for an Interface Between Electromagnetic Transient and Phasor Solutions", Accepted to present in *2015 IEEE 10th International Conference on Industrial and Information Systems (ICIIS)*, December 17-20 2015, Peradeniya, Sri Lanka.

7.3 Future Work

A natural extension of this work would be to improve the model to achieve a numerically stable simulation for a larger network.

Another extension of this work would be to develop a small signal model for the entire system (including the SRF-PLL, EMT modelled network and the dynamic phasor equivalent) and perform a sensitivity analysis on the eigenvalues. This will help to understand the reasons for instability in the EMT-DP hybrid model.

References

[1] Jos Arrillaga Neville Watson. Power systems electromagnetic transients simulation. 39, 2003. doi: 10.1049/PBPO039E.

[2] U.D. Annakkage, N.C. Nair, A.M. Gole, V. Dinavahi, T. Noda, G. Hassan, and A. Monti. Dynamic system equivalents: A survey of available techniques. In *Power Energy Society General Meeting, 2009. PES '09. IEEE*, pages 1–5, July 2009. doi: 10.1109/PES.2009.5275650.

[3] TURHAN HILMI DEMIRAY. *Simulation of Power System Dynamics using Dynamic Phasor Models*. PhD thesis, SWISS FEDERAL INSTITUTE OF TECHNOLOGY, ZURICH, 2008.

[4] Xi Lin. *System Equivalent for Real Time Digital Simulator*. PhD thesis, University of Manitoba, Canada, 2010.

[5] A.S. Morched, J.H. Ottevangers, and L. Marti. Multi-port frequency dependent network equivalents for the emtp. *Power Delivery, IEEE Transactions on*, 8(3):1402–1412, July 1993. ISSN 0885-8977. doi: 10.1109/61.252667.

[6] M. Abdel-Rahman, A. Semlyen, and M.R. Iravani. Two-layer network equivalent for electromagnetic transients. *Power Delivery, IEEE Transactions on*, 18(4):1328–1335, Oct 2003. ISSN 0885-8977. doi: 10.1109/TPWRD.2003.817749.

[7] P. Triverio, S. Grivet-Talocia, M.S. Nakhla, F.G. Canavero, and R. Achar. Stability, causality, and passivity in electrical interconnect models. *Advanced Packaging, IEEE Transactions on*, 30(4):795–808, Nov 2007. ISSN 1521-3323. doi: 10.1109/TADVP.2007.901567.

[8] T. Demiray, G. Andersson, and L. Busarello. Evaluation study for the simulation of power system transients using dynamic phasor models. In *Transmission and Distribution Conference and Exposition: Latin America, 2008 IEEE/PES*, pages 1–6, Aug 2008. doi: 10.1109/TDC-LA.2008.4641716.

[9] A.M. Stankovic and T. Aydin. Analysis of asymmetrical faults in power systems using dynamic phasors. *Power Systems, IEEE Transactions on*, 15 (3):1062–1068, Aug 2000. ISSN 0885-8950. doi: 10.1109/59.871734.

[10] H. Konara and U.D. Annakkage. Evaluation of two positive sequence filters for an interface between electromagnetic transient and phasor solutions, accepted to present. In *2015 IEEE 10th International Conference on Industrial and Information Systems (ICIIS)*, December 2015.

[11] C. Dufour, J. Mahseredjian, and J. Belanger. A combined state-space nodal method for the simulation of power system transients. *Power Delivery, IEEE Transactions on*, 26(2):928–935, April 2011. ISSN 0885-8977. doi: 10.1109/TPWRD.2010.2090364.

[12] P. Forsyth, R. Kuffel, R. Wierckx, Jin-Boo Choo, Yong-Beum Yoon, and Tae-Kyun Kim. Comparison of transient stability analysis and large-scale real time digital simulation. In *Power Tech Proceedings, 2001 IEEE Porto*, volume 4, pages 7 pp. vol.4–, 2001. doi: 10.1109/PTC.2001.964822.

[13] The fiber enhanced backplane is here!–rtds technologies inc. `https://www.rtds.com/the-fiber-enhanced-backplane-is-here/`, Accessed: 2015-10-05.

[14] A.M. Stankovic, P. Mattavelli, V. Caliskan, and G.C. Verghese. Modeling and analysis of facts devices with dynamic phasors. In *Power Engineering Society Winter Meeting, 2000. IEEE*, volume 2, pages 1440–1446 vol.2, 2000. doi: 10.1109/PESW.2000.850191.

[15] Sebastian Henschel. *Analysis of electromagnetic and electromechanical power system transients with dynamic phasors*. PhD thesis, The University of British Columbia, Canada, February 1999.

[16] Chandana Karawita. *HVDC Interaction Studies Using Small Signal Stability Assessment*. PhD thesis, University of Manitoba, Canada, April 2009.

[17] Xuegong Wang, P. Wilson, and D. Woodford. Interfacing transient stability program to emtdc program. In *Power System Technology, 2002. Proceedings. PowerCon 2002. International Conference on*, volume 2, pages 1264–1269 vol.2, 2002. doi: 10.1109/ICPST.2002.1047605.

[18] L. A. Snider H. Su, K. W. Chan and J-C. Soumagne. Advancements on the integration of electromagnetic transients simulator and transient stability simulator. In *International Conference on Power Systems Transients Montreal*, January 2005.

[19] A Ghoshal and J. A Vinod. Method to improve pll performance under abnormal grid conditions. In *National Power Electronics Conference 2007. Indian Institute of Science, Bangalore*, 2007.

[20] EdwardA. Lee and DavidG. Messerschmitt. Phase-locked loops. In *Digital Communication*, pages 700–724. Springer US, 1994. ISBN 978-1-4684-0006-9. doi: 10.1007/978-1-4684-0004-5_15. URL `http://dx.doi.org/10.1007/978-1-4684-0004-5_15`.

[21] V. Kaura and V. Blasko. Operation of a phase locked loop system under distorted utility conditions. *Industry Applications, IEEE Transactions on*, 33 (1):58–63, Jan 1997. ISSN 0093-9994. doi: 10.1109/28.567077.

[22] Ping Hsu and M. Behnke. A three-phase synchronous frame controller for unbalanced load [invertor operation]. In *Power Electronics Specialists Conference, 1998. PESC 98 Record. 29th Annual IEEE*, volume 2, pages 1369–1374 vol.2, May 1998. doi: 10.1109/PESC.1998.703214.

[23] Wu W-Y et al. Guo X-Q. Phase locked loop and synchronization methods for grid-interfaced converters: a review. 2011. doi: R.87NR4/2011.

[24] Xiaoming Yuan, J. Allmeling, W. Merk, and H. Stemmler. Stationary frame generalized integrators for current control of active power filters with zero steady state error for current harmonics of concern under unbalanced and distorted operation conditions. In *Industry Applications Conference, 2000. Conference Record of the 2000 IEEE*, volume 4, pages 2143–2150 vol.4, Oct 2000. doi: 10.1109/IAS.2000.883122.

[25] Sang-Joon Lee, Jun-Koo Kang, and Seung-Ki Sul. A new phase detecting method for power conversion systems considering distorted conditions in power system. In *Industry Applications Conference, 1999. Thirty-Fourth IAS Annual Meeting. Conference Record of the 1999 IEEE*, volume 4, pages 2167–2172 vol.4, 1999. doi: 10.1109/IAS.1999.798754.

[26] M. Karimi-Ghartemani and M.R. Iravani. A method for synchronization of power electronic converters in polluted and variable-frequency environments. *Power Systems, IEEE Transactions on*, 19(3):1263–1270, Aug 2004. ISSN 0885-8950. doi: 10.1109/TPWRS.2004.831280.

[27] Cheng-Che Chen and Yuan-Yih Hsu. A novel approach to the design of a shunt active filter for an unbalanced three-phase four-wire system under

nonsinusoidal conditions. *Power Delivery, IEEE Transactions on*, 15(4):1258–1264, Oct 2000. ISSN 0885-8977. doi: 10.1109/61.891512.

[28] M. Karimi-Ghartemani. A novel three-phase magnitude-phase-locked loop system. *Circuits and Systems I: Regular Papers, IEEE Transactions on*, 53 (8):1792–1802, Aug 2006. ISSN 1549-8328. doi: 10.1109/TCSI.2006.879057.

[29] Se-Kyo Chung. A phase tracking system for three phase utility interface inverters. *Power Electronics, IEEE Transactions on*, 15(3):431–438, May 2000. ISSN 0885-8993. doi: 10.1109/63.844502.

[30] Balarko Chaudhuri Bikash Pal. Robust control in power systems. 2005. ISBN 978-0-387-25950-5.

[31] A.M. Gole and V.K. Sood. A static compensator model for use with electromagnetic transients simulation programs. *Power Delivery, IEEE Transactions on*, 5(3):1398–1407, Jul 1990. ISSN 0885-8977. doi: 10.1109/61.57982.